Analytical Methods

RSC Publishing

CRITICAL REVIEW

View Article Online
View Journal | View Issue

Cite this: *Anal. Methods*, 2013, **5**, 1098

Electrochemical impedance spectroscopy: an overview of bioanalytical applications

Edward P. Randviir and Craig E. Banks*

Received 30th November 2012
Accepted 9th January 2013

DOI: 10.1039/c3ay26476a

www.rsc.org/methods

The application of electrochemical impedance spectroscopy (EIS) has increased dramatically in the past few years due to its ability to elucidate a plethora of physical and electronic properties of electrochemical systems such as diffusion coefficients, electron transfer rate constants, adsorption mechanisms, charge transfer resistances, capacitances and pore sizes. This review provides a short introduction to the fundamental principles of EIS before exploring the many exciting and pertinent analytical applications regarding the numerous methods in biosensing, the application of EIS with graphene based materials and last, the use of EIS with screen printed electrodes.

1 Introduction

Electrochemical Impedance Spectroscopy (EIS) is a technique which has been utilised by many institutions for over a century[1,2] for purposes such as corrosion analysis,[3,4] adsorption properties of molecules (interfacial behaviour)[5,6] and also used to monitor the functioning of batteries and fuel cells[7,8] amongst many other applications. The technique is based upon complex mathematical transforms first described in the late 19th century by Oliver Heaviside to yield real values of impedance in temporal space. As a respected mathematician, Heaviside is also credited with the invention of terminologies such as impedance,[9] admittance and conductance.[10] Critically, he defined the 'operational impedance' as the "complex ratio of the voltage and current in an AC circuit",[11,12] which is denoted today as:

$$Z(j\omega) = \frac{V(j\omega)}{I(j\omega)} \quad (1)$$

where Z is the impedance, V is the voltage, I is the current, j is the imaginary component and ω is the frequency. The

Faculty of Science and Engineering, School of Chemistry and the Environment, Division of Chemistry and Environmental Science, Manchester Metropolitan University, Chester Street, Manchester M1 5GD, Lancs, UK. E-mail: c.banks@mmu.ac.uk; Web: www.craigbanksresearch.com; Fax: +44 (0) 1612476831; Tel: +44 (0) 1612471196

Edward P. Randviir studied chemistry at the University of Hull where he graduated with a first class with honours MChem with Nanotechnology. He is in the second year of study towards his Ph. D. with the Banks' research group at Manchester Metropolitan University where his current focus is the application of electrochemical impedance spectroscopy to biological systems and the comparison to other electrochemical techniques including cyclic voltammetry. Aside from his electrochemical roots, Edward has various scientific interests, the most notable being surfactant and colloid science.

*Craig E. Banks is an Associate Professor of Chemistry at Manchester Metropolitan University and has published over 220 papers with a h-index over 38 (*Web of Science*, Jan 2013). He has written 4 books, contributed 11 book chapters and is an inventor of 15 patents. Craig has also spun out two companies from his research. Craig was awarded the Harrison–Meldola Memorial Prize in 2011 for his contributions to the understanding of carbon materials, in particular graphene and its application as an electrode material. His current research is directed towards the pursuit of studying the fundamental understanding and applications of nano-electrochemical systems such as graphene, carbon nanotube and nanoparticle derived sensors and developing novel electrochemical sensors* via *screen printing and related techniques.*

subsequent development of impedance in relation to diffusional electrochemical systems (discussed later) was first reported by Warburg in 1899[1] and the principles have been implemented increasingly to the present day to the point where EIS has now branched away from universities and into industry for quality control purposes (paints, emulsions, corrosion).[11] In fact, almost any process which changes the conductivity of a system can be recognised by EIS, hence a multitude of properties can be elucidated using the technique.

A common approach in electrochemistry is the application of layers of chemicals, polymers, or coatings to electrodes (known as composite electrodes) which provide useful enhancements in terms of electron transfer and sensitivity. The effects of these different layers and coatings can be identified using EIS,[13,14] including electrochemical contributions from polar, ionic and dielectric relaxation processes[11] in the electrolyte system as well as within the electrode, at the electrode surface and within the double-layer region. Exchange-current densities, charge-transfer resistances, double-layer capacitances,[15] and other key parameters of an electrochemical system under investigation can also be measured. EIS can also be used to estimate physical parameters such as surface roughness and the porosity of an electrode.[16]

The use of EIS in biological applications has also apparently been reported since as early as 1925.[11] One of the first reported uses of EIS in these applications estimated the overall impedance of biological cells,[17] and has more recently been utilised to study the activity of enzymes combining with target molecules.[18] The technique is now widely reported in bioanalytical applications as a result of the many years of work in developing the technique; in fact, biological applications cover the majority of EIS research today as we will see later. It is clear that there is a large volume of information available to the researcher and hence explains why the use of EIS is increasing rapidly as more is learnt about the technique.

The purpose of this review is to focus upon the latest developments of EIS, including (less so) non-biological and (more so) biological applications, which usually focus upon certain bio-recognition events (antigen–antibody binding) in conjunction with composite electrodes. Many researchers use EIS as a tool to back up their electrochemical ideas and do not offer rigorous explanation of EIS data and in effect use EIS as a tool to confirm ideas (such as electrode composite characterization) which are subsequently investigated using techniques such as cyclic voltammetry, differential pulse voltammetry and square wave voltammetry, and thus this article will hopefully, where possible, focus upon work which has used EIS as their main strategy for investigation. The article will start by briefly explaining some of the fundamental concepts surrounding EIS which are essential for the user to be able to understand first how to set up an EIS experiment, and second the methods used to interpret the data obtained in EIS spectra, and will continue to apply these concepts to, and discuss, current literature regarding non-biological and biological applications of EIS, examine how composite electrodes are utilized in EIS experiments, and last discover the potential applications of screen printed electrodes for electroanalytical purposes.

2 Fundamental principles

In principle, impedance is simply the opposition force to electrical current in a circuit and is measured in the same units as resistance, Ω.[19] However resistance differs from impedance because resistance obeys Ohm's law, and is observed in DC circuits where the resistance is technically the impedance with zero phase angle, since the current is not alternating. The concept of resistance can only be applied in an AC circuit if certain criteria are met: (i) the AC voltage and current must be in phase with each other; (ii) the resistance is frequency-independent; and (iii) the resistance can be applied to all currents and voltages. Unfortunately in the vast majority of cases the phase angle is not equal to zero, as capacitative and/or inductive effects are observed at almost all frequencies (*vide infra*), hence a more general principle must be used to account for frequency-dependence; the concept of impedance essentially allows a quantitative representation of the opposition force to electrical current in these cases (as in AC circuits).

In the majority of EIS experiments (as in AC polarography[11]), a fixed sinusoidal voltage is applied by a potentiostat across a 3 electrode cell containing (normally) a solution of electrolyte harboring the molecule under investigation. The amplitude and load (*viz.* magnitude of the voltage) of the fixed sinusoidal voltage should be dependent upon the type of molecular system under investigation;[20] biological molecules tend to be subject to smaller voltages than non-biological ones as the structures of the biological molecules are easily denatured this way. Another method of assembling an EIS experiment (and in particular for use within biological applications) is to construct a composite upon the electrode surface which will attract target analytes and thus affect the conductivity of the system through either a blocking or a 'molecularly wired' admittance mechanism. In most cases where this strategy is applied, impedance measurements are performed in a blank buffer solution or a known redox probe (such as potassium ferricyanide(II)[21] or hexamine-ruthenium (III) chloride[22]) after the composite and target analyte have been assembled upon the electrode surface. Subsequently when the load is applied at a set frequency, a current will flow through the electrochemical cell which is recorded by the potentiostat and converted by the software *via* eqn (1) into an impedance value with a real and imaginary component. This process is repeated across a frequency range where different values are deduced for the real and imaginary components of the overall impedance value.

EIS, as discussed previously, requires manipulation of complex numbers to deduce true values for the impedance. This is achieved by the software in which the user selects to obtain impedance spectra; Solartron Analytical[23] and Ivium[24] are examples of such companies offering EIS equipment and the relevant software. The data can be presented in a variety of ways, for instance real and imaginary impedance components are plotted against one another in Nyquist plots (Fig. 1) which have to be interpreted properly to deduce solution resistances, charge transfer resistances and Warburg impedance as well as time constants, whereas in Bode plots, the impedance and phase angle is plotted against frequency which can be helpful to

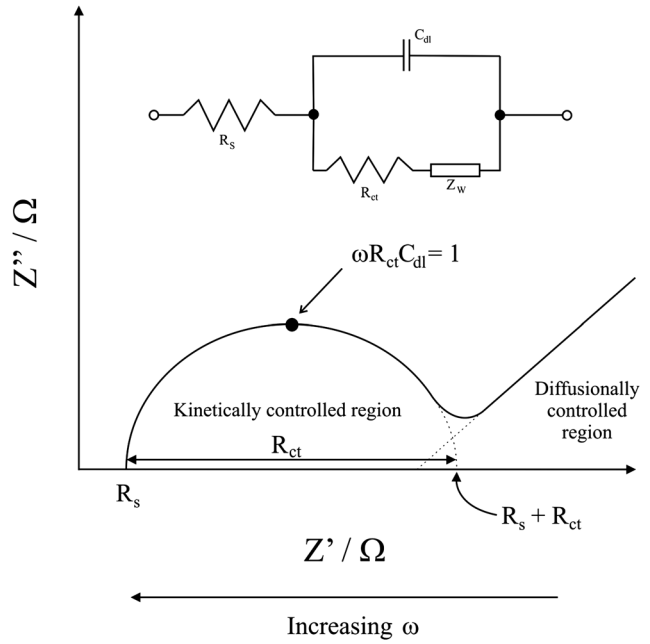

Fig. 1 Simple Randles equivalent circuit for an electrochemical cell. Reproduced from ref. 10 with permission from Elsevier.

find capacitative or inductive effects of electrochemical systems. Note Nyquist plots will be referred to in this review more extensively than other forms of graphical EIS representation. For further information on Bode plots, see Scully and Silverman.[25]

Two fundamental equations (eqn (2) and (3)) describe the real and imaginary impedances of the most common representation of an EIS experiment, the Nyquist plot (an example of a Nyquist plot is shown in Fig. 1):

$$Z' = R_S + \frac{R_{ct}}{1 + \omega^2 {R_{ct}}^2 {C_{dl}}^2} \quad (2)$$

and

$$Z'' = \frac{{R_{ct}}^2 C_{dl} \omega}{1 + \omega^2 {R_{ct}}^2 {C_{dl}}^2} \quad (3)$$

where Z' and Z'' are the observed impedance due to the real and imaginary parts, respectively, R_s is the solution resistance, R_{ct} is the charge transfer resistance, ω is the angular frequency and C_{dl} is the double layer capacitance. Further, values of capacitance and inductance are related to current and voltage *via* eqn (4) and (5):

$$I = CV \quad (4)$$

$$I = V/L \quad (5)$$

where I is the current, C is the capacitance, V is the voltage, and L is the inductance. Hence, the impedance function, Z, can be written in terms of capacitance or inductance *via* eqn (6) and (7):[11]

$$Z = \frac{1}{\omega C} \quad (6)$$

$$Z = \omega L \quad (7)$$

An Ohm's law-like relationship can be used to calculate the total impedance of a circuit with numerous components, as is seen in EIS circuits, by simply taking the sum of the impedances of each component (provided the impedance components are in series):[11]

$$Z_{total} = Z_1 + Z_2 + Z_3 \ldots Z_x \quad (8)$$

EIS circuits are often simplified into circuit diagrams to benefit the user in helping understand the different components contributing to the overall impedance of the circuit and also are used for computer simulations of impedimetric systems. For instance, in an electrochemical experiment, impedance will arise from the solution resistance (R_s), double layer charging at the electrode surface (C_{dl}), charge transfer resistance (R_{ct}), and the so-called Warburg Element (Z_w) as depicted inset in Fig. 1. The combination of these elements is known as a Randles circuit;[26] such circuits are habitually used to simulate EIS experiments. Naturally, most cases are far more complex than this. For instance factors like adsorption changes impedance so must be accounted for as well as enzyme binding (*i.e.* bio-recognition) and electrode composites for example.

The Warburg Element accounts for the diffusion of the ions in solution in an electrochemical reaction. For instance at high frequencies, Warburg impedance is not observed as migration occurs over much longer time periods than the operational frequency and thus the relatively slow movement of molecules in solution renders impedance contributions to be obsolete. Hence, Warburg contributions are generally seen in the low frequency region; the right hand side of Fig. 1 illustrates the diffusional controlled region of a Nyquist plot obtained using EIS. The solution resistance is independent of the frequency and is observed in Fig. 1 at the highest frequency where the real axis is intersected (R_s). The charge transfer resistance (R_{ct}) is the opposition experienced to electron movement and is a real quantity. R_{ct} is observed in Fig. 1 at the second extrapolated intersection with the real axis in the mid- to low-frequency region; this region is marked as the kinetically controlled region of the Nyquist plot in Fig. 1, and is related to the heterogeneous electron transfer rate constant, k^0, by following eqn (9):

$$R_{ct} = \frac{RT}{F^2 k^0 C} \quad (9)$$

for a simple one electron process where R is the molar gas constant, T is the temperature, F is the Faraday constant and C is the concentration of the electroactive species.

The double layer capacitance (C_{dl}) can be roughly estimated from Fig. 1 by the Z''_{max} of the semi-circle. Recent authoritative work by Wang and Pilon has explained that the capacitances measured using EIS at low frequency are unreliable at best, with the paper quoting some literature reporting EIS capacitances exhibiting a 20% discrepancy.[27,28] Furthermore, the value of the habitually quoted RC circuits by electrochemists is questioned in work by Rubinson and Kayinamura who state (on the modelling of RC circuits) "*the overall impedance expressions corresponding to most models give little or no direct information*

about the physical meaning of the elements for such models".[29] The capacitative element of an electrochemical cell is often represented by a constant phase element (CPE) which, simply put, accounts for factors which affect the capacitance of a system like surface inhomogeneities resulting in differing reaction rates upon the surface which introduces multiple time constants.[30] CPE's are discussed in a recent review by Dominguez-Benetton *et al.*[31]

To demonstrate the applicability of EIS, we refer to work by Sluyters and Oomen (1960)[11,32] who estimated the electron transfer rate constant of the $Zn(Hg)/Zn^{2+}$ couple in a 1 M $NaClO_4$ and 1 mM $HClO_4$ electrolyte at a hanging mercury drop cell.[32] The frequency range selected was 20 Hz to 20 kHz (probably due to the limited progression of electronics) and observed in this frequency range was a single semi-circle on a Nyquist plot, characteristic of near-ideal charge transfer resistance (see Fig. 2). Interpretation of Fig. 2 reveals the solution resistance, (depicted as R_∞), to be approximately 800 Ω and is easily attainable simply by observing the first intersection of the semicircle with the real axis. The semi-circle is extrapolated in the mid- to low-frequency region to the real axis to reveal $R_2 + R_\infty$, which is an estimate of the sum of the charge transfer resistance and the solution resistance. Note in this review, R_2 shall be referred to as R_{ct}. The R_{ct} is estimated to be *ca.* 2500 Ω. This method of estimating the R_{ct} is used almost ubiquitously amongst the electrochemical field. From the R_{ct}, estimated from the Nyquist plots from a range of concentrations of Zn^{2+} ions, the authors have estimated the electron transfer rate constant, k^0, of the $Zn(Hg)/Zn^{2+}$couple to be 3.26×10^{-3} cm s^{-1} (±3.6%) *via* the following equation:[11,33]

$$R_{ct} = \frac{RT}{n^2F^2k^0\left(C_{Zn^{2+}}\right)^{\alpha}\left(C_{Zn(Hg)}\right)^{1-\alpha}} \quad (10)$$

where n is the number of electrons transferred. Note eqn (10) is an adaptation of eqn (9), accounting for the number of electrons transferred being more than 1. For a potential where the electrode reaction is governed totally by the electron transfer kinetics for a simple one electron process:

$$R_{ct} = \frac{RT}{i_0F} \quad (11)$$

where i_0 is the exchange current density as given by:

$$i_0 = Fk^0C \quad (12)$$

Clearly the sheer amount of information from one plot can make EIS a difficult, perhaps daunting, and time consuming technique in terms of interpretation, however as we will see, the use of EIS is increasing and becoming ever more applicable to the needs of modern day society.

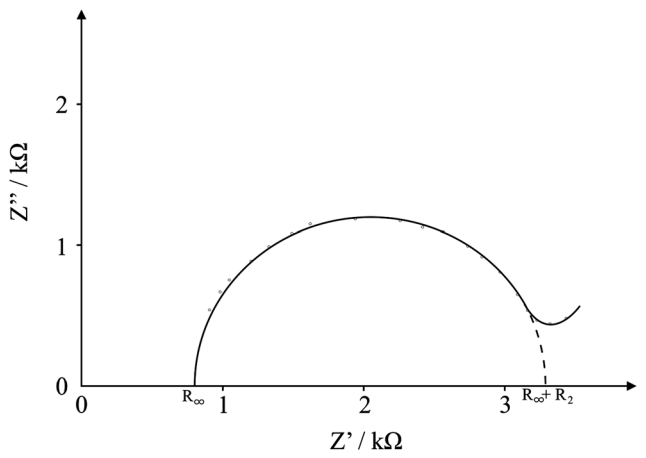

Fig. 2 Nyquist plot which illustrates the frequency-dependent impedance characteristics of a $Zn(Hg)/Zn^{2+}$ couple. The circles are approximate experimental data values; the line is a best-fit line to illustrate the required parameters for investigation. Redrawn from ref. 32 with permission from Wiley.

3 EIS in non-biological applications

As mentioned in the introduction, EIS is a technique commonly utilised for observing corrosion of metals and monitoring the degradation of paints and emulsions, and also in monitoring the performance lithium-ion cells. This section very briefly highlights the non-biological applications of EIS and recent developments.

Probably the most common employment of EIS is the monitoring of corrosion upon metallic surfaces. It is well known that the level of corrosion upon a metal surface is related to the current which can flow through the metal in the absence of an external electric field, and the phenomenon is aptly named the 'corrosion current';[34] this phenomenon was initially exploited in the early 1970's to measure the extent corrosion at a metal–water–air interface. In fact, the circuitry in ref. 34 was meticulously designed to measure the ionic conductor resistance across a pair of electrodes which were to be subjected to a DC voltage.[34] There is no doubt that the design revolutionised the way corrosion is measured, however given that it is resistance being measured and not total impedance, and the fact that the circuitry also feeds AC signals to elucidate voltage and current readings,[34] results are basically ideal and as discussed in the introduction, impedance is dependent on the frequency, *i.e.* in an AC circuit. Subsequently, researchers turned to impedance measurements to deduce corrosion rates at metallic surfaces.

An elegant review by Epelboin *et al.* published in 1972[35] summarises the known methods for the detection of corrosion at surfaces (such as the plotting of current–potential curves and the measurement of double-layer capacities) before suggesting impedance as a tool for the measurement of corrosion.[35] Their review describes how the most useful entity for the measurement of corrosion rate is in fact the so-called 'transfer resistance' which the review defines as the extent of faradaic impedance at infinite frequency.[35] The suggestion that transfer resistance is the most adequate method of measuring corrosion is rationalised by the fact that the transfer resistance is a purely resistive quantity and therefore less variables affect transfer resistance (given that it is frequency-independent). For a mathematical evaluation of corrosion rates, see Epelboin *et al.*[35]

The use of EIS was later implemented for the detection of corrosion on metals coated with polymer coatings as early as 1973 by Menges and Schneider[36] who plotted the impedance modulus against the applied frequency as a function of exposure time to nitric acid on polymer coatings applied to steel.[36] Many years have passed since the publication of the authoritative review,[35] and many more developments in EIS technology have naturally been reported.

Presently EIS is being used to study corrosion for use in a plethora of applications. First, we briefly touch upon the application to dental treatments. For instance, Mareci *et al.*[37] have utilised EIS to study the corrosion resistances of dental alloys in an artificial saliva[38] which is reportedly approximately pH 5.6.[37] Note the use of EIS in dental alloy studies has been known for over a decade; a well cited paper on this area of research is by Pan *et al.*, who conducted work on titanium alloys in biological environments.[39] Resuming to the work by Mareci *et al.*,[37] their EIS experiments utilising an alloy named Vera-BondB (which comprises of 12.7% Cr, 9% Mo, 1.95% Be, 2% Al and the rest Ni) showed that at short immersion times in biological environments the impedance is far lower than that of long immersion times, showing that the alloy in question exhibits a high level of inactivity after exposure for 1 week to artificial saliva. Furthermore, their studies showed that higher Cr percentage made the alloy more noble and hence more favourable to be used as an alloy for use in dental treatment.

Other recent corrosion work has been reported by Xue *et al.*, who have used EIS to investigate corrosion rates of magnesium alloys for use as biodegradable implants for medicinal purposes.[40] Their paper describes how the main obstacle which prevents magnesium based implants is the fast degradation rates associated with current magnesium implants as described by Song *et al.*[40,41] Xue *et al.* effectively try to increase the corrosion resistance of the magnesium alloy magnesium–yttrium (Mg–4Y) by applying a coating comprising of water-based 1,2-bis-triethoxysilyl ethane (BTSE) silane which is dispersed in a water containing epoxy resin upon the Mg–4Y working electrode and use EIS to measure the corrosion resistance.[40] Fig. 3 illustrates the Nyquist plots obtained from their EIS experiments conducted in subcutaneous tissue on mice, and it is clear to see that the resistance of the bare Mg–4Y material in Fig. 3A has increased upon the addition of the epoxy BTSE silane in Fig. 3B. This increase of resistance eludes to the Mg–4Y biological implant design exhibiting a longer lifetime due to a higher resistance to corrosion.[40] Furthermore, their studies also found that the implants exhibited *higher* corrosion resistances *in vivo* rather than *in vitro* (conducted in simulated bodily fluid) and hence the work holds potential for development of implants which degrade slowly and are not harmful to the human body.[40]

Another interesting non-biological application of EIS focuses upon the monitoring of lithium-ion and fuel cells. The monitoring of interior degradation is very important for electrochemical devices, mainly for safety purposes *i.e.* prevention of leakage and exposing toxic substances to the atmosphere or worse to human beings. With lithium-based batteries being recalled from shop shelves in 1991,[42] researchers had to redirect their work towards the design of safer batteries for the general public. Lithium-ion batteries provided a solution and researchers continue to pursue them today. In particular, lithium metal phosphates attract a considerable amount of attention from researchers due to the compounds being apparently highly safe.[43]

In the case of lithium-ion cells, many institutions focus upon modifying the lithium electrode to enhance the electrode transfer kinetics and use EIS to monitor this.[44–46] For instance, Liu *et al.* created a fast-ion conductor, $Li_{2.8}(V_{0.9}Ge_{0.1})_2(PO_4)_3$, using a solid state reaction applied upon a steel conducting plate of which the electron transfer kinetics were studied using EIS using a lithium-based electrolyte.[44] Their work shows high frequency impedance contributions ascribed to ion migration through the applied lithium-based surface films as well as

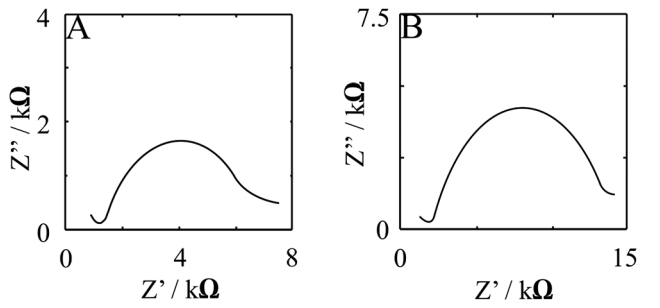

Fig. 3 Nyquist plots of (A) Mg–4Y working electrode and (B) working electrode coated with epoxy BTSE silane conducted in subcutaneous tissue on mice. Adapted from experimental data taken from ref. 40 with permission from Elsevier.

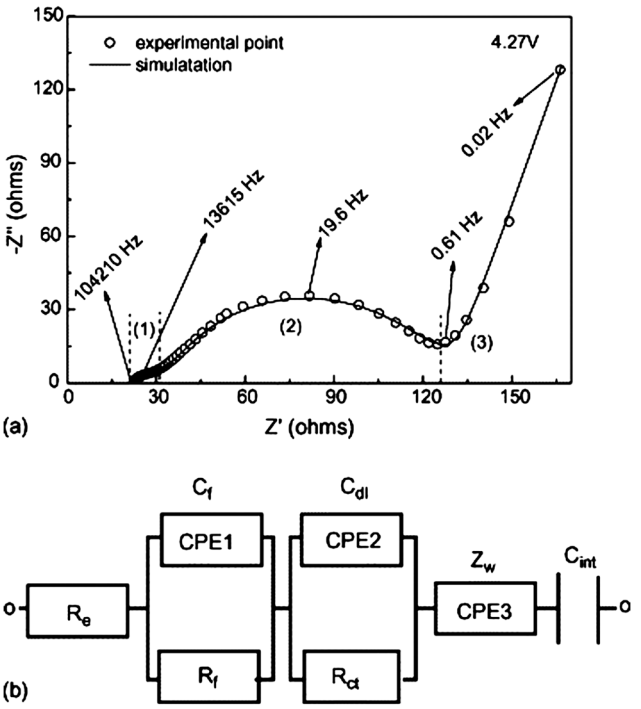

Fig. 4 (a) The impedance response of $Li_{2.8}(V_{0.9}Ge_{0.1})_2(PO_4)_3$ at 4.27 V during first charge cycle and its fitting with the equivalent circuit. (b) Equivalent circuit used to fit the experimental data. Reproduced from ref. 44 with permission from Elsevier.

diffusion and charge transfer.[44] Depicted in Fig. 4 is a Nyquist plot of the $Li_{2.8}(V_{0.9}Ge_{0.1})_2(PO_4)_3$ from their work, which has been held at a potential of +4.27 V. The circles are experimental data and the line is the simulated data using the proposed equivalent circuit in Fig. 4b. The high frequency domain (1) shows a small perturbed semi-circle of which the authors attribute to ion migration through the $Li_{2.8}(V_{0.9}Ge_{0.1})_2(PO_4)_3$ surface film. The mid-frequency range (2) semi-circle is proposed to be of a result of charge transfer in the system. Note the mid-frequency range in a Nyquist plot, similar to the Bode plot, describes the level of capacitance of the system but as mentioned previously, is not considered to be accurate. The sloped area in the low-frequency region (3) is a result of the diffusion of the system[44] and is called the Warburg impedance, Z_w, a component in Fig. 4b. Other components in Fig. 4b are the resistance from the cell and electrolyte, R_e, the resistance of the surface film, R_f and C_f (described as a constant phase element, CPE1, to account for non-ideal capacitative behaviour), charge transfer resistance, R_{ct} and C_{dl} (CPE2), and the so-called accumulated capacitance, C_{int}. The authors estimate the diffusion coefficient of the Li^+ ions in the electrochemical system to be 10^{-8} to 10^{-7} cm^2 s^{-1} (dependant on holding potential) by using:[44,47]

$$R_e(Z_W) = \sigma_W \omega^{-\frac{1}{2}} \quad (13)$$

and

$$D_{Li^+} = \frac{1}{2}\left[\left(\frac{V_m}{FA\sigma_W}\right)\left(-\frac{dE}{dx}\right)\right]^2 \quad (14)$$

where V_m is the molar volume, D_{Li^+} is the diffusion coefficient of the lithium ions, F is the Faraday constant, A is the electrode surface area, σ_W is the Warburg factor (Warburg element), E is the applied potential and x is the concentration of the species under investigation. Eqn (13) is implemented to deduce the Warburg element; the gradient of a plot of Z' and Z'' *vs.* $1/\omega^2$ is equal to σ_W which can then be substituted into the eqn (14) as all the other terms are known. The values deduced for the diffusion coefficient, by comparison to the authors previous work, show "*excellent diffusion performance*"[44] on the basis that previous diffusion coefficients for other materials were estimated to be one order of magnitude slower.[48] This example highlights how diffusion coefficients (and subsequently electron transfer coefficients) can be estimated by use of EIS. Note reproducible surfaces are required for high quality EIS results (*vide supra*), hence the use of surface film methodologies have to be carefully implemented to ascertain reliable results. Further, it is known that the underlying electrode affects electrochemical measurements when surface coatings are applied, and as in this case, the underlying is steel which can corrode, potentially introducing more parameters.

Other work by Yan *et al.* have used a lithium metal phosphate film in an attempt to improve the performance of lithium-ion batteries.[43] Unlike Liu *et al.*, who experimented with different cation ratios for lithium-ion performance,[44] Yan *et al.* vary the anion ratio in the sol–gel synthesized $Li_3V_2(PO_4)_{3-x}Cl_x$/C.[43] The working electrodes were fabricated in-house in conjunction with polytetrafluoroethylene (PTFE), as opposed to the film technique discussed previously. EIS of the electrodes in a lithium-based electrolyte ($LiPF_6$) was conducted to estimate the diffusion coefficients of several variations of anion content by varying the value of the anion stoichiometry, x. This is illustrated in Fig. 5 as a series of Nyquist plots. For an un-doped $Li_3V_2(PO_4)_{3-x}Cl_x$/C sample, the semi-circle is large which alludes to a large charge transfer resistance, which decreases as the working electrode material is further doped with anions. The authors believe that the increase in anion doping stimulates electrochemical activity of the lithium in the $Li_3V_2(PO_4)_{3-x}Cl_x$/C complex which increases conductivity and subsequently decreasing the charge transfer resistance.[43] The diffusion coefficient is estimated to be 5.78×10^{-10} ($x = 0.12$) through the use of eqn (15):[43]

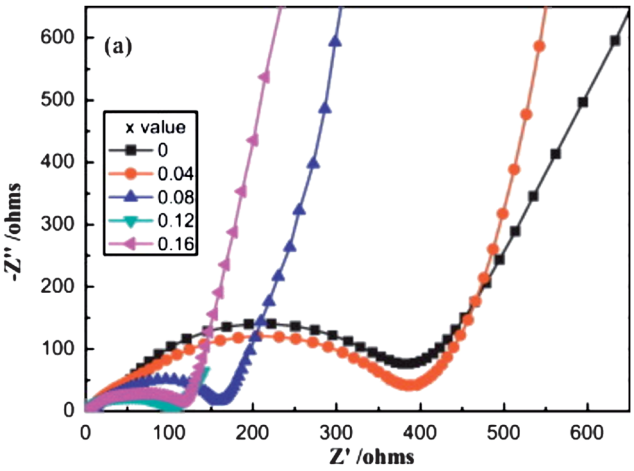

Fig. 5 Nyquist plots for the electrochemical impedance measurements of the $Li_3V_2(PO_4)_{3-x}Cl_x$/C electrode in a lithium-based electrolyte. Note the value of x is the stoichiometric ratio of Cl in the electrode. Reprinted from ref. 43 with permission from Elsevier.

$$D = \frac{R^2T^2}{2A^2n^4F^4C^2\sigma^2} \quad (15)$$

where R is the molar gas constant, T is the absolute temperature, A is the surface area of the working electrode, n is the number of electrons transferred, F is the Faraday constant, C is the concentration and σ is the Warburg factor, which is calculated from eqn (13). In comparison to the previous example, the diffusion rate is 3 orders of magnitude slower with the anionic doping method in these given examples;[43,44] note this should not be assumed to be a general rule. It is also worthy of note that the two examples use different equations to derive their diffusion coefficients.

Another parameter which is extremely useful and can be elucidated *via* EIS is the exchange current density of an electrochemical cell, which is essentially the net current of an electrochemical cell in the absence of an external electrical field (or basically at zero overpotential, assuming there is no other electrical influence). This parameter is a key part of a lithium-ion EIS study conducted by Wang *et al.*[14] In their work, they calculate the exchange current density, j_0, *via* the charge transfer resistance taken from a Nyquist plot. Wang *et al.* utilise

eqn (16) to estimate the exchange current densities of various lithium-containing compounds where j_0 is the exchange current density, A is the surface area of the electrode, R is the molar gas constant, T is the absolute temperature, n is the number of electrons exchanged in the electrochemical reaction, F is the Faraday constant, and R_{ct} is the charge transfer resistance.[14]

$$j_0 = \frac{i_0}{A} = \frac{RT}{nFR_{ct}A} \quad (16)$$

Further, they introduce the concept of surface film resistance in a quantitative fashion, observed as double semi-circles in their EIS spectra. That is, the diameter of the semi-circle of the proposed surface film contribution on the Nyquist diagram corresponds to the surface-film resistance (readers are referred to ref. 14 for further insights).[14]

So far we have shown how EIS can be utilised to monitor corrosion resistance and to estimate diffusion coefficients within lithium ion cells to gain insights into their performance. Further uses for non-biological applications include proton exchange membrane fuel cells (PEMFCs). Given that today's PEMFCs do not operate efficiently under extreme conditions (low humidity, high temperatures *etc.*), research has been on-going for many years to improve the efficiency of PEMFCs under these conditions.[7] EIS is a technique which is used to monitor newly designed substrates for PEMFCs, and has been rigorously reviewed by many people, including Zhang and co-workers in 2007 (ref. 49) and 2008,[50] by He and Mansfield in 2009,[8] and more recently, Borole *et al.*[51] have rigorously investigated the effect of the charge transfer resistances in biological systems in microbial fuel cells (MFCs) utilising EIS over long periods of time.

This section has, hopefully, delivered a concise collection of work regarding the non-biological applications of EIS for the reader to refer to when conducting experiments on corrosion and lithium-ion cells; interested readers should consult the literature where there are hundreds of journal articles regarding these topics highlighting the importance of this application area, and have not been mentioned because this review focuses largely upon the biological applications of EIS which are more specifically directed towards the sensing applications of EIS to combat real world problems. The next section shall discuss these highly relevant biological applications of EIS including biosensing and DNA detection.

4 EIS applied to biological systems

To this point, the review has covered fundamental principles associated with EIS, and has also explored some pertinent non-biological applications of EIS including corrosion detection, electrochemical activity of lithium ion cells and monitoring fuel cell performance. This section will assess the plethora of biological applications utilising EIS and overview the range of information which can be extrapolated from EIS in biological applications. It is worthy of note that work by Samanta and Sarkar[52] reviews literature regarding the immobilisation of biomacromolecules upon substrates and discusses the relative merits of the different methodologies applied; such techniques are commonplace from this point forward.

Firstly, EIS has been used in the development of DNA biosensors. An example of the use of EIS in the detection of DNA damage is a paper by Hlavata *et al.*[53] In their work, screen printed carbon electrodes (SPE) are utilised which is rarely seen in the literature for the case of EIS. A composite is applied to the surface of the SPE, consisting of single walled carbon nanotubes (SWCNT), which are known to be beneficial for the detection of DNA,[54] chitosan (CHIT) obtained from shrimp shells (normally

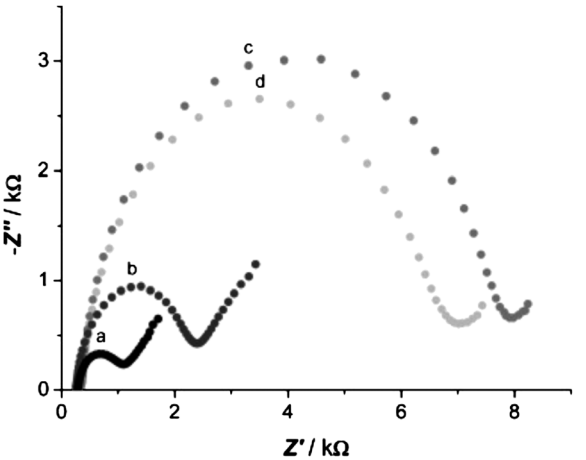

Fig. 6 Nyquist plots in the presence of 1×10^{-3} mol L^{-1} $[Fe(CN)_6]^{3-/4-}$ in 0.1 mol L^{-1} PBS of pH 7.0, potential 0.1 V *vs.* Ag-SPE/AgCl, frequency range 0.1–5000 Hz, potential amplitude 10 mV: (a) no thioridazine present in the solution, measured at the SWCNT–CHIT/SPCE; (b) 1×10^{-7} mol L^{-1} thioridazine present in the solution, measured at the SWCNT–CHIT/SPCE; (c) no thioridazine present in the solution, measured at the DNA/SWCNT–CHIT/SPCE; (d) 1×10^{-7} mol L^{-1} thioridazine present in the solution, measured at the DNA/SWCNT–CHIT/SPCE. Reproduced from ref. 53 with permission from Elsevier.

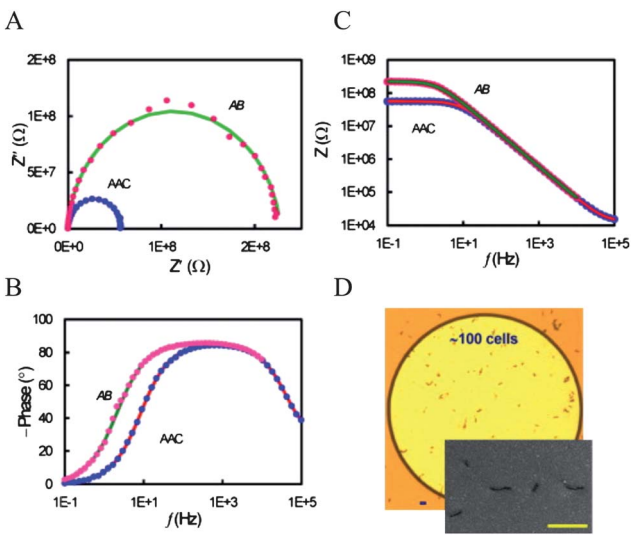

Fig. 7 (A–C) Nyquist, Bode phase and Bode modulus plots (dotted curve-experimental and solid curve-fitted) obtained after antibodies and casein blocker (AAC) and after bacteria capture (AB). (D) The optical and SEM (inset) images of *E. coli K12* captured on the microelectrode. The electrolyte used is 5 mM $Fe(CN)_6^{3-/4-}$ in 0.01 M PBS buffer. The antibody and bacteria concentration is ~50 μg mL^{-1} and ~1.0×10^7 cfu mL^{-1}, respectively. The scale bar in (D) is 3 μm and 8 μm (inset). Republished from ref. 55 with permission from Elsevier.

used as a blood clotting agent), and the DNA which has a known base sequence.[53] A Nyquist plot comparing different electrode modifications in 1 mM $[Fe(CN)_6]^{3-/4-}$ is shown in Fig. 6, where it can be seen that the addition of the SWCNT and CHIT on the electrode surface increases the charge transfer resistance which appears as a larger semi-circle in the plot.[53] Comparing (c) to (d), where the difference is only that the electrolytic solution in (c) contains no DNA binding agent (thioridazine) and (d) contains the binding agent, there is a small change in the charge transfer resistance. This is ascribed to the binding agent combining with the DNA on the electrode surface and hence acting as a molecular wire, stimulating electron transfer, increasing conductivity and hence reducing charge transfer resistance.[53] The figure is not accompanied with an equivalent circuit yet we can speculate from the previous examples and taking into account the shape of the Nyquist plot. First, given the shape of the plot, with a semi-circle and a small linear section, we would expect a simple Randles circuit in the frequency range tested with a small contribution from the Warburg impedance (which would be more prevalent if the frequency range extended to lower frequencies). Surprisingly though, no small semi-circle is observed in the high frequency range which we might expect given the composite upon the electrode. This could be because the impedance of the film is extremely small, which is a valid conclusion given that carbon nanotubes exhibit fast electron transfer. It would be preferable to enlarge the high frequency range to observe any impedance contribution from the film.

A recent development of the use of biological substrates in tandem with EIS concerns label-free biosensors,[55] which have been studied for over a decade in conjunction with EIS.[56,57] We focus upon recent work by Siddiqui *et al.*,[55] who have undertaken the difficult challenge of interpreting the antibody-antigen binding mechanism by rigorous interpretation of EIS in conjunction with ultrananocrystalline diamond (UNCD) microelectrode arrays. Their work firstly shows that the attachment of antibodies to an electrode surface introduces a charge transfer resistance to the system, whereas the bare UNCD electrodes, rather than exhibiting charge transfer, show only diffusional components in their corresponding impedance spectra.[55] Further, upon introduction of *E. coli* to the electrode *via* a specific binding mechanism to the corresponding antibody upon the electrode surface, the overall impedance increases further.[55] The impedance spectra for these observations are depicted in Fig. 7. The solid lines on the impedance spectra represent simulations from a proposed equivalent circuit (not reported here) and are in excellent agreement with the obtained experimental data. The circuit rationalises the impedance contributions exhibited from both the deposited surface antibody matrix, casein, and the UNCD microelectrodes which are called pores (basically arising from inhomogeneities from the deposition of the matrix upon the electrode surface). Turning attention to Fig. 7A, it is observed that after the bacteria is bound to the antibody, AB, the semi-circle in the Nyquist plot has increased massively compared to the case of the antibody only, AAC, which shows an increase in the charge transfer resistance. According to the authors[55] this happens due to the bacteria being a large molecule which blocks the electrode surface even more so than the antibody which has been deposited upon the surface which is intuitive.

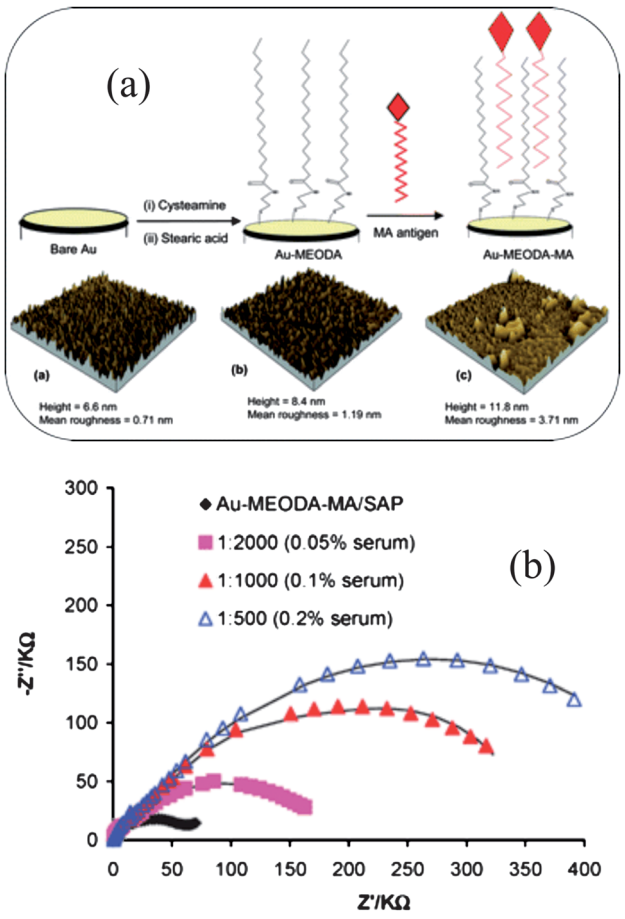

Fig. 8 (a) Schematic diagram depicting the application of the antigen to the electrode surface and; (b) EIS spectra of the modified electrodes at differing serum concentrations. Reprinted from ref. 58 with permission from the Royal Society of Chemistry.

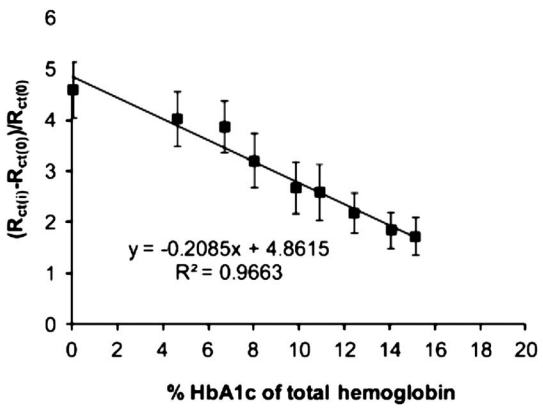

Fig. 9 The calibration plot corresponding to the change of electron transfer resistance of the immunosensor with the concentration of HbA1c. The *y*-axis depicting charge transfer resistance is reported as the charge transfer resistance with the analyte, $R_{ct(i)}$, minus the charge transfer resistance without the analyte (essentially background), $R_{ct(0)}$, divided by $R_{ct(0)}$. Reproduced with permission from ref. 60 with permission from the Royal Society of Chemistry.

Table 1 An overview of the recent and pertinent biological applications of EIS

No.	Electrode	Sensing element	Detection limit	Notes	Ref.
1	GCE/Pty/Au/Pt_{NP}[a]	PEP DNA[b]	3.6×10^{-13} M	Au/Pt nanoparticles formed on film surface *via* electrodeposition	105
2	CNT/CHIT/PGE[c]	Hepatitis B	13.25 μg mL^{-1}	Electrode characterization only	106
3	GCE/CNT/PEI/Do[d]	NADH	3×10^{-6} M	Surface oxides formed from dopamine act as a redox mediator for NADH	107
4	Ab2-HRP/Ag/Ab1/GR-MWCNT/GCE[e]	Human IgG[f]	0.2 ng mL^{-1}	Method based on immunoassay. Labour intensive	108
5	Au/Cx5s/MCE[g]	Cocaine	0.1 μM	Near linear increase in impedance with the logarithm of cocaine concentration, ($R^2 = 0.98$)	109
6	Hg^{2+} specific DNA films on Au	Hg^{2+}, Pb^{2+}	1 pM, 0.1 pM	Increased admittance exhibited as the ions improve conductivity[h]	110
7	GCE	Acetaminophen	—	Linear regression of concentration *vs.* R_{ct} with $R^2 = 0.9889$. Claims that GCE is a good bare electrode for sensing purposes	111
8	Au-SAM[i]	*E. Coli*	—	Label-free method for the detection of *E. Coli* with appropriate control experiments	112
9	Au microelectrode arrays[j]	Cortisol	1 pM	Potential for wireless health monitoring, non-invasive and monitoring can take place when the subject is asleep	113
10	Glucose oxidase on gold	Glucose	39 mg dL^{-1}	Potentially increase the sensitivity of glucose sensing for diabetes applications	114
11	Gold screen printed electrodes modified with a thiolated antibody	Wound infection biomarkers[k]	1.1 nM	Conducted in 'mock wound fluid'	115
12	InvA-gene based electrode composite	Salmonella	0.5 pM	Complex electrode fabrication involving polymerase chain reaction (PCR)	116
13	DNA modified gold electrode	Breast cancer gene, BRCA1	0.05 nM	Exonuclease used to cleave double stranded DNA upon the electrode surface, the leftover ssDNA used to bind to the target DNA	117
14	Gold electrode modified with relevant aptamer	B-estradiol (sex hormone)	2 pM	Concentration studies found a linear increase in charge transfer resistance with increasing concentration	118
15	ITO composite electrode[l]	Trace water in organic solvents	0.65 ppm	Termed a 'microgap impedance sensor'	119
16	ssDNA and gold nanoparticles on a gold electrode	Chronic lymphocytic leukemia	1 pM	Highly selective, sensitive, and fast detection towards the sequence-specific DNA for leukemia	120
17	Interdigiated microelectrodes coated with indium tin oxide	Salmonella	10^2 to 10^4 cfu mL^{-1}	Salmonella detection in milk samples.	121 and 122
18	Functionalised gold electrode[m]	Rhodopsin	10 ng mL^{-1}	Work is aimed at developing a biosensor for detection of retinal proteins	123
19	Conducting polymer film[n] on GC	Vitellogenin	0.42 μg L^{-1}	Authors claim their sensor can be considered as an alternative to the laborious ELISA technique	124
20	Gold nanoparticles and aryl diazonium salts on gold electrodes	Anti-biotin IgG	5 ng mL^{-1}	Apparent sensitive and selective platform for detection of large molecules	125
21	Stainless steel	Food pathogens	10^5 cfu mL^{-1}	2 Electrode system utilized. Long data collection times	126
22	Self-assembled monolayers on gold[o]	Human IgG	2–10 μg mL^{-1}	Impedance signal amplified by a protein – streptavidin network on the electrode surface which made the detection limits lower	127
23	Modified graphite electrode[p]	Amylase in saliva	—	Potential for label-free biochips according to the authors	128
24	Nanostructured polycarbonate substrate[q]	Der p2[r]	0.1 pg mL^{-1}	Extremely low detection limit reported	129
25	Pt[s]	Xanthine	0.1 mu M	The electrode was used for determination of xanthine in fish meat when in storage	130
26	Pt/yttria stabilized zirconia	Oxygen (partial pressures)	—	τ is inversely proportional to the pressure	131
27	Gold composite electrodes[t]	Cobalt ions	10^{-9} M	Highly sensitive polymeric cobalt sensors	132

Table 1 (*Contd.*)

No.	Electrode	Sensing element	Detection limit	Notes	Ref.
28	Molecularly imprinted polymers	Urea/creatine	10 ng mL^{-1}/40 ng mL^{-1}	Good selectivity	133
29	Au/SiO_2/Si in a PVC membrane	Zinc ions	10^{-8} M	Highly sensitive	134
30	Gold interdigitated electrodes upon a glass substrate	Organo-phosphorous compounds	1 pM	A potential application for the detection of these toxic class of compounds which are found in pesticides	135
31	Anti-C-reactive protein upon nanocrystalline diamond	C-reactive protein[u]	10 nm	Highly sensitive label-free immunosensor	136
32	DNA monolayers on gold.	Simultaneous detection of lead, silver and mercury ions	10 pM, 10 nm, and 0.1 nm, respectively.	Claims to be a cost effective sensor that has been tested in lake water and calf serum.	137
33	Propargyl-funtionalised ferrocene upon gold	Ascorbic acid	2.6 pmol L^{-1}	Sensor successfully applied to detect ascorbic acid in urine samples	138
34	Gold interdigitated electrodes on a glass substrate	Monoclonal mouse IgG, sarcosine, lead sulfide	pM range	Combines EIS with microfluidics	139 and 140
35	Nanocrystalline diamond	Human IgE[v]	0.03 μg mL^{-1}	Linear relationship between capacitance and IgE concentration	141
36	Graphene oxide modified GCE	Rabbit IgG antibody	0.67 nM	Functionalisation of hydroxide groups on graphene oxide utilized to tailor electrode to specific needs	142
37	Screen printed carbon electrodes	Gold nanoparticles	—	A method is devised to characterize the diameters of the gold nanoparticles	143
38	Gold microelectrodes functionalized with an amino thiol and carbon nanotubes	D-dimer[w]	0.1 pg mL^{-1}	Development of rapid point-of-care analysis for deep vein thrombosis	144
39	Modified gold electrode[x]	Food borne mycotoxin	0.08 ng dL^{-1}	Sensor has 30 s response time	145
40	RNA composite upon gold	Hepatitis C	~800 000[y] IU mL^{-1}	Amplification required for better detection limits	146

[a] Pty – polytyramine; Au-Pt_{NP} – gold–platinum nanoparticles. [b] Phosphoenolpyruvate carboxylase. [c] Single-walled carbon nanotube-chitosan modified pencil graphite electrode. [d] Multiwalled carbon nanotubes modified with dopamine functionalized polyethylenimine upon a glassy carbon electrode. [e] Horseradish peroxidase conjugated goat anti-human IgG (Ab2-HRP), goat anti-human IgG (Ab1), chemically reduced graphene (GR), multi walled carbon nanotube (MWCNT). [f] Human immunoglobulin. [g] Gold electrode modified with specific aptasensor for cocaine binding (Cx5s), which has been chemically thiolated to self-assemble onto the gold electrode, and subsequently treated with mercaptoethanol (MCE). [h] An impedance sensing model seldom seen. [i] α-Mannoside self-assembled upon a gold electrode with a thiolated spacer to reduce steric hindrance. [j] Arrays modified with dithiobis (succinimidyl propionate) self-assembled monolayer. [k] Namely TREM-1 (Triggering Receptor-1 Expressed on Myeloid cells), MMP-9 (Matrix MetalloPeptidase 9), and HSL (*N*-3-oxo-dodecanoyl-L-HomoSerineLactone). [l] Composite consists of PDMDAAC (poly(dimethyldiallylammonium chloride)) and ferro/ferricyanide. [m] Gold electrodes are functionalized with goat IgG and an anti-rhodopsin antibody. [n] Conducting polymer film made by cycling the electrode between 0 V and +1.6 V in a 0.1 M solution of tetrabutylammonium perchlorate/dichloromethane with 1 mM 5,2′:5′2″terthiophene-3′-carboxylic acid dissolved in. [o] Thioctic acid assembled on gold before addition of the antibody. [p] Graphite electrode is held at a fixed potential of −0.2 V in an acetate buffer containing 3-hydroxyphenylacetic acid for 60 seconds, before being held at the same potential for 60 seconds in acetate buffer containing anti-human saliva alpha-amylase (anti-HSAf) which acts as the binder for the amylase. [q] Polycarbonate mold was created using a nickel template, which was then 'sputtered' with gold to create a thin gold film upon the substrate before electrodeposition of gold nanoparticles to create a monodisperse layer. [r] Der p2 = dust mite antigen. [s] Zinc oxide nanoparticles/chitosan/MWCNT/polyanilineand xanthine oxidase upon platinum. [t] Polyvinylchloride and polymethylhydrosiloxane were the polymers used for the film, which incorporated a macro-cyclic molecule, calix-6-arene, into the structure. [u] C-reactive protein is produced in the liver and is highly prevalent when inflammation of a part of the body occurs.[147] [v] Human immunoglobulin E. [w] D-dimer is a molecule associated with deep vein thrombosis. [x] Gold electrode modified with 11-amino-1-undecanethiol which harbours anti-ochratoxin-A antibodies. [y] By the article's own admission, the reported units for their instrumentation are generally unknown and no conversion factors are reported. IU = international unit.

However simple this may sound, it is only a recent development in the interpretation of impedance data and for use in electroanalysis. The next example is also a similar type of impedance model.

More exciting work concerning antibody–antigen recognition has been conducted by Mathebula *et al.*[58] who have used EIS for the detection of tuberculosis (TB). In their article they report a novel method to self-assemble an antigen layer upon a gold electrode.[58] First, a layer of a long-chain organic compound (*N*-(2-mercaptoethyl)octadecanamide, MEODA) is assembled upon the electrode surface by firstly immersing the electrode in cysteamine before adding stearic acid.[58] The electrode is then incubated in a solution of dry dimethylformamide (DMF) containing mycolic acids (MA) for 48 hours.[58] The process is depicted in Fig. 8a. Note the mycolic acids are the antigens which act as the recognition molecules for the TB.[58] The electrodes were then immersed in saponin (SAP) which is a blocking agent, utilised in this case to block all non-specific adsorption/binding sites and hence the impedance measurements taken after the TB binding step can be assumed to be a result of the bound TB. These electrodes were then used in EIS experiments on human sera which were HIV and TB positive ($HIV^{+}TB^{+}$) and negative ($HIV^{-}TB^{-}$) as their study is focused upon combating TB in HIV/TB co-infected individuals as TB is the biggest killer for HIV infected individuals.[58,59] Fig. 8b illustrates their EIS data as a result of the TB binding to the antibody at the electrode surface and shows clearly that the charge transfer resistance increases as the concentration of TB is increased compared to the electrode which has not been subject to $HIV^{+}TB^{+}$ immersion.[58] This work highlights how useful EIS could potentially be for the medicinal technologies.

Further work involving the use of antibodies has been described by Liu *et al.*[60] who have devised a method to implement EIS electroanalytically for the detection of HbA1c a type of haemoglobin which is used to elucidate the concentration of glucose in blood plasma.[60] Their method is based on a concept named "competitive inhibition assay" where in this case the HbA1c and the antibody are suspended together in a series of sera in which the HbA1c concentrations are varied. The competitive inhibition derives from the fact that the percentage of antibody adsorbed to the electrode composite is dependent on the amount of antibody complexing with the HbA1c;[60] in other words the higher the concentration of the HbA1c, the less antibody available for adsorption to the electrode composite, and thus the charge transfer resistance will decrease compared to lower concentrations of HbA1c as, intuitively, there is less material blocking the flow of electrons through the electrochemical cell. The resultant experiments show a negative correlation between HbA1c concentration and charge transfer resistance, illustrated in Fig. 9 in the form of a calibration plot[60] which is required in analytical applications. This calibration plot could potentially be used for glucose detection for diabetics and hospital patients. Though there are already many glucose detection technologies available, the pursuit of more accurate results is always desired by scientists; EIS could provide that solution. At least, the detection limits for such experiments are extremely low; refer to Table 1 for more information.

Other recent work in biological applications includes: the impedimetric detection of Myoglobin by Wang *et al.*,[61] though their use of a 205 mV holding potential for biological applications should be questioned as there is potential for denaturation; electrochemical detection of morphine and diclophenac in pharmaceutical samples by Mokhtari *et al.*;[62] and work by Santos *et al.*[63] which focuses upon the electron transfer mechanisms of horseradish peroxidase (HRP) immobilised upon a glassy carbon electrode with nafion and polymyxin in a diffusionless system with a view to understanding the electron transfer mechanisms of this particular enzyme. Interestingly, the latter example loosely links charge transfer resistance to electron-hopping between the iron centre of the HRP and target molecules such as O_2 and H_2O_2.[63] The evidence to support this is cycling their composite electrode 500 times in O_2 saturated media and measuring the impedance which is compared to the impedance of a bare glassy carbon electrode. It is found that the charge transfer resistance decreases with cycling in this particular electrochemical system[63] which they believe is due to a slow electron transfer rate between the enzyme and the O_2 which has been suggested previously by Venarusso *et al.*[64] EIS has also recently been utilised by Prats-Alfonso *et al.* for the use of detection and quantitative measurement of p53-antibodies,[65] which are used in medicinal technologies as prognostic indicators for ovarian cancer and biomarkers for other types of cancer.[65] In a quantitative context, the authors use EIS to detect said antibodies to a *picomolar* concentration,[65] which demonstrates that the technique of EIS can be, in some cases, extremely sensitive. For further examples regarding electrochemical aptamer-based biosensors (pre-2011) we refer the reader to a review by Ferapontova and Gothelf.[66]

5 EIS with graphene composite electrodes for biological sensing applications

The use of graphene-based derivatives in electroanalysis has accelerated over the past few years; especially since the Nobel Prize for physics was awarded to Geim and Novoselov in 2010[67] for the fabrication and characterisation of single layer graphene.[64,68] Graphene has also been a topic of interest within our own research group, though has rarely seen success in terms of beneficial electrochemical responses which could be utilised for sensing applications in its pristine form (defined later).[69] For example, graphene has been shown to reduce the overpotential required for the electrochemical oxidation of guanine which could be classed as beneficial,[70] yet more often than not it has also been shown to perturb the electrochemical response of known electroactive biologically relevant analytes such as ascorbic acid and NADH.[71] Note the aforementioned examples were conducted with pristine graphene which is a commercially available near single-layer graphene that, unlike other commercially available graphenes, is free from any electroactive surfactants or intercalated impurities exhibiting perceived electrocatalysis which can be confused with graphene possibly exhibiting beneficial electrocatalytic effects.[72] Note also graphene is a relatively young area of research regarding electrode modification. For more information about electrode modification per se methodologies, see Bard

(1983)[73] and for specific information about self-assembled monolayers, see Bain,[74] Nuzzo[75] or Porter.[76]

Given the use of graphene-based derivatives in modern electrochemistry, this section focuses mainly upon graphene utilised in conjunction with EIS for biological applications, as well as carbon nanotubes[77,78] and other carbon-based electrode composites such as nanoporous carbon,[79] as they are widely reported by researchers attempting to find more solutions for everyday problems and applications in electroanalysis. Note the current volume of literature regarding graphene and EIS is comparably low to the other topics covered within this review and is perhaps the reason why current graphene-based EIS reviews are substantially lacking in content.[80] Despite this, the current literature in this area focuses upon DNA analysis, biosensing and immunoassays – a review by Bonanni *et al.* offers an excellent schematic representation of a generic graphene/biomolecule impedance setup.[80] We shall see that graphene and EIS are used together to detect a wide scope of analytes, from MRSA[81] to proteins associated with Alzheimer's disease.[82]

A fine example (and indeed to our knowledge, the first of its kind in terms of a graphene-based impedimetric DNA sensor) of graphene-based impedimetric sensing is reported by Bonanni and Pumera who apply so-called "hairpin" DNA oligomers (with a complimentary base sequence to that of Alzheimer's disease) to graphene-coated electrodes.[83] They report that upon immersion into a solution containing DNA oligomers with the complimentary base sequence (hybridized), the R_{ct} of the redox probe potassium ferrocyanide decreases compared to a non-immersed electrode (non-hybridized).[83] The authors attribute the decrease in R_{ct} to the hybridized DNA strands desorbing from the electrode surface, a claim which is unsubstantiated within their work *i.e.* there is no electrode surface characterization pre- and post-experiment.[83] Nevertheless the work represents a new sensing platform for such diseases. Graphene-based apta- and immuno-sensors have also been developed by the same group.[84,85]

However, the following example bucks the trend of graphene uses being reported only within the bioanalytical field (at least, where impedance measurements are concerned). Very recently, graphene has been proposed as a novel material to coat metallic surfaces with a view to reducing corrosion and the experiments conducted by Raman *et al.* utilise EIS as a means to study this effect.[86] Copper sheets were engineered and washed with deionised water and acetone prior to experiments. The EIS experiments were conducted in 0.1 M NaCl using a frequency range of 1 MHz to 10 MHz.[86] Fig. 10 illustrates Bode plots obtained for uncoated and graphene coated copper in 0.1 M NaCl and it is clear from Fig. 10a that the impedance at high frequencies is far higher for the graphene coated copper than it is for the uncoated copper.[86] In fact, the impedance is almost 2 orders of magnitude larger for the graphene coated copper compared to the uncoated copper. This work is somewhat novel, considering previous efforts to coat metals with graphene have yielded improved corrosion resistances, but only twice that of the uncoated metal,[87] albeit in a different electrolyte.

Graphene has also been formed *in situ* for use as anodic coatings in microbial fuel cells;[88] another non-biological

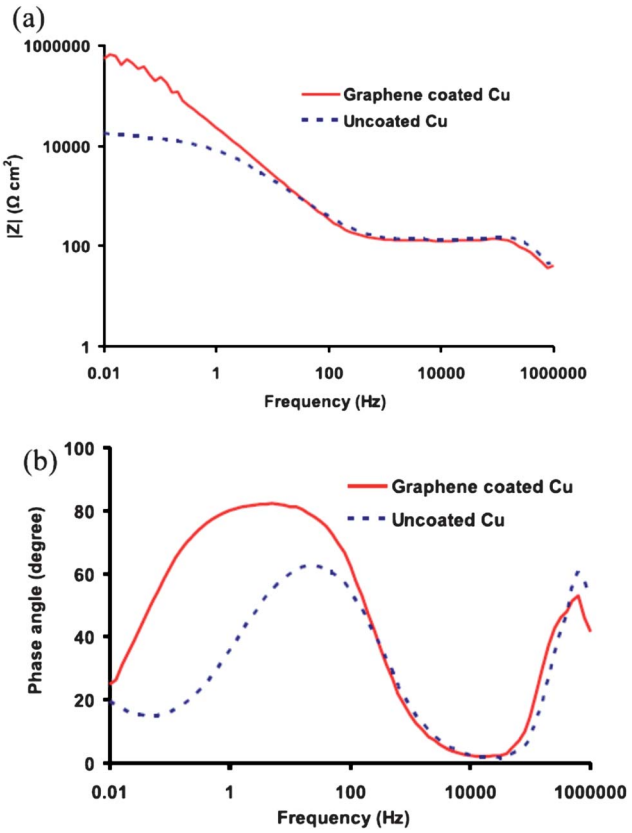

Fig. 10 Bode plots of the uncoated and graphene coated copper: (a) impedance modulus and; (b) phase angle. Reprinted from ref. 80 with permission from Elsevier.

graphene application of EIS. Note previous studies have utilised carbon nanotube networks in biofilms for the same purpose, yielding positive results in terms of decreased fuel cell resistance.[89] A graphene network was formed in the biofilm on the fuel cell's anode by mixing graphene oxide with acetate and injecting the solution into a well-used microbial fuel cell (MFC) whose voltage output was less than 50 mV. The solution was later replaced by acetate. A graphene network was subsequently formed by microbial reduction of graphene oxide in the biofilm and characterised by SEM imaging which showed the networks formed upon the anodes were that indeed of graphene.[88] According to the authors, EIS measurements of the anodes revealed charge transfer resistances to decrease by approximately half upon the addition of the graphene scaffold to the biofilm thus suggesting the graphene scaffold increases the conductivity of the system.[88]

Turning attention back to graphene uses in biological applications, we focus upon work by Hu *et al.* who describe a "label-free electrochemical DNA hybridization assay using functionalized graphene as a platform."[90] Modern technologies for the sensing of DNA require label-free, fast, and non-destructive techniques for analysis and have been studied by many groups as well as our own.[70] EIS and voltammetric techniques currently lead the way in label-free DNA sensing, however EIS offers a wealth of information regarding changes at the surface of the electrode composites as well as possible DNA

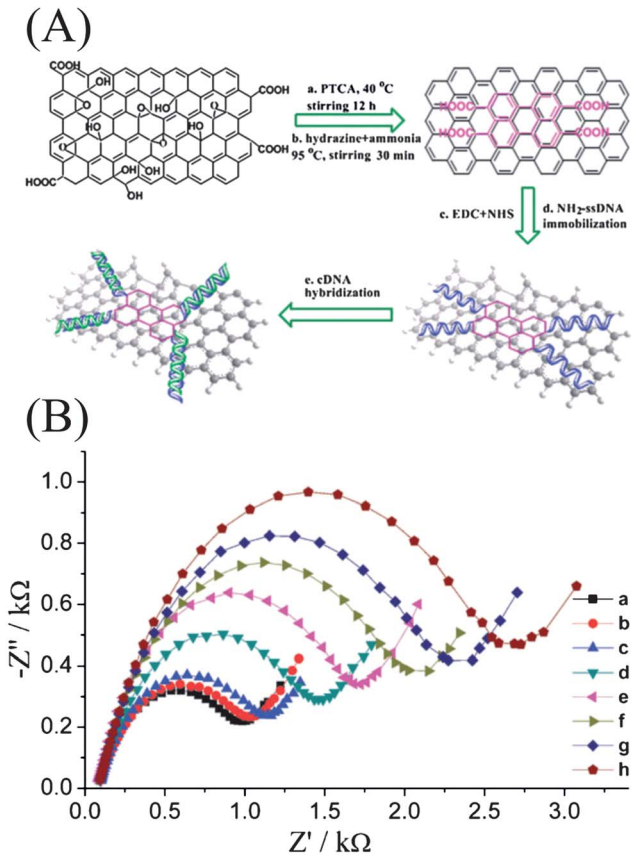

Fig. 11 Schematic diagram (A) of the formation of the graphene/PTCA network and the ssDNA binding step; and EIS data for the graphene/PTCA/ssDNA composite (B) in solution of differing concentrations of pol gene: without hybridization (a) and after hybridization with its complementary HIV-1 pol gene sequences of different concentrations: 1.0×10^{-12}, 1.0×10^{-11}, 1.0×10^{-10}, 1.0×10^{-9}, 1.0×10^{-8}, 1.0×10^{-7} and 1.0×10^{-6} M (b–h). Adapted from ref. 84 with permission from Springer.

strand conformation changes.[90] Hu *et al.* construct a composite comprising of graphene and 3,4,9,10-perylene tetracarboxylic acid (PTCA), which is used as a platform to immobilise single stranded DNA (ssDNA), shown in Fig. 11a.[90] The advantage in this case of immobilising ssDNA with a known base sequence is that a target ssDNA strand with the complementary base sequence can selectively bind to the ssDNA upon the surface which clearly will have an effect upon the observed spectra obtained *via* EIS. In the case of Hu *et al.* the complimentary target molecule is the pol gene of the *human immunodeficiency virus-1* (HIV-1).[90] A pol gene is simple to use as it is a retrovirus that encodes its reverse transcriptase enzyme. Fig. 11b shows the effect of the increase in concentration of the pol gene on the Z' and Z'' components of EIS, and it is apparent that the charge transfer resistance increases as the concentration of pol gene increases.[90] Furthermore, control experiments were conducted utilising mismatched DNA strands of differing base sequences, all of which exhibited lower transfer resistances than the pol gene and thus less binding to the ssDNA at the surface. Unfortunately, the paper doesn't conclude their impedimetric bioassay by plotting R_{ct} *vs.* concentration which would have been useful to assess whether the technique could be incorporated into electroanalysis.[90] However, inspection of Fig. 11b would suggest at least a gradual, if not linear, increase in R_{ct} as the concentration of pole gene present increases.

Further recent advances in graphene technology carry on with the theme of sexually transmitted diseases, and concern the electrochemical detection of the *Neisseria gonorrhoea* bacterium which is responsible for the sexually transmitted disease gonorrhoea.[91] A chemically prepared polyaniline and iron oxide nanocomposite is deposited upon an indium tin oxide electrode in the work by Singh *et al.* which, upon addition of an amino labelled DNA probe, selectively exhibited an increased charge transfer resistance when immersed in a solution of complimentary DNA taken from gonorrhoea bacteria.[91] Comparably, the total impedance was found to be larger than when the electrode was immersed in *K. Pneumoniae*, *S. Aureus*, *E. Coli* or *N. Sicca*.[91] This work suggests that graphene related composites could be utilised to create miniaturised sensing platforms to selectively detect different strains of bacteria and (hopefully) concentration levels. It is an exciting prospect to think that disease could be diagnosed on-the-spot instead of taking extended periods of time by sending samples to labs and using time consuming techniques such as PCR and ELISA.

Finally, using similar EIS methods to those described previously in this section, Wang *et al.* devise a method incorporating graphene oxide for the impedimetric detection of the

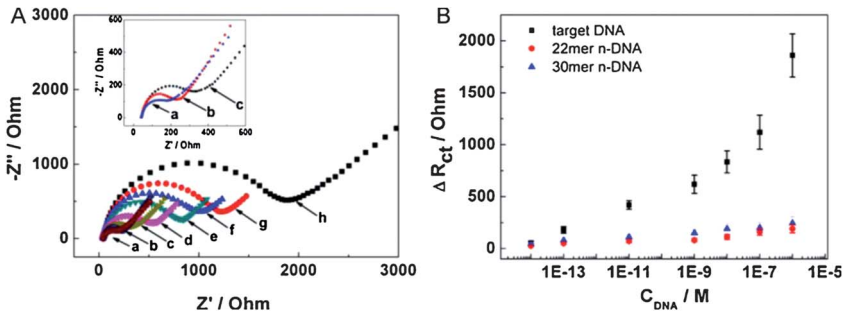

Fig. 12 (A) Nyquist plots of GCE-APTES-rGO-ssDNA hybridized with target DNA at different concentrations: (a) 0, (b) 10^{-14}, (c) 10^{-13}, (d) 10^{-11}, (e) 10^{-9}, (f) 10^{-8}, (g) 10^{-7} and (h) 10^{-6} M. Inset: magnification of curves a, b and c. (B) The plot of R_{ct} *vs.* logarithm of the concentration of target DNA (squares), 22mer n-DNA (circles), and 30mer n-DNA (triangles), respectively. Frequency range: from 0.1 to 100 000 Hz; electrolyte: 5 mM $[Fe(CN)_6]^{3-/4-}$ (1 : 1) in 0.01 M phosphate buffer solution (pH 7.4) containing 0.1 M KCl; amplitude: 5 mV. Adapted from ref. 78. Copyright (2011) of The American Chemical Society.

infamous methicillin-resistant *Staphylococcus aureus* (MRSA) DNA.[81] Similar to previous graphene examples, they specifically design their electrodes in a manner which connects the graphene to the surface *via* chemical linkage; they used 3-aminopropyltriethoxysilane (APTES) as a molecule to link the graphene oxide to the glassy carbon surface as described in their previous work.[92] Note readers are referred to ref. 92 for more information on the electrode preparation. To prepare the DNA containing electrode, they simply employ the drop-casting method by which they pipette 50 μL of the relevant ssDNA upon the surface and leave to dry in closed humid conditions for 6 hours. Next, varying concentrations of the complimentary DNA were applied to the electrode surface for 30 minutes. The electrodes were subsequently washed with PBS to remove any loosely bound material. Control experiments were conducted using non-complimentary DNA (22 and 30 base sequence DNA labelled 22mer and 30mer). EIS experiments took place in 0.01 PBS (pH 7.4) with 0.1 M KCl.[81] The EIS data obtained concluded that the concentration of the MRSA complimentary DNA largely affected the charge transfer resistance; highlighted in Fig. 12.[81] Fig. 12B is a clear indication that the MRSA binds to the electrode as the charge transfer resistances are far larger than the random DNA fragments used in the control experiments. Hence, the method has potential use for the label-free detection of the deadly bacteria[81] and has the advantage of being quick and relatively cheap.

6 EIS in conjunction with Screen Printed Electrodes

Screen Printed Electrodes (SPEs) are disposable electrodes which can be specifically tailored for the detection of target analytes;[93] we have already seen an example earlier on where SPEs are used with EIS (refer to Section 4). SPEs are specifically useful because of disposability, the lack of need of surface pretreatment before and during measurements, reduced sample size required for analysis (~<20 μL) and their scale of economics due to the ability to be mass produced. SPEs also exhibit excellent reproducibility (<5%, depending on the system) within and between batches, highlighted by incorporation into sensors for diabetics to measure their blood glucose on-the-spot. However, currently the use of SPEs is practically limited to voltammetric techniques and the direction of research focuses upon tailoring analyte specific SPEs,[94] and the use of novel electrode geometries such as microelectrode SPEs,[95] and screen printed microelectrode arrays[96] for the voltammetric determination of target analytes. This section shall subsequently briefly explore the current literature regarding SPEs for use with EIS which surprisingly are almost incongruous with one another in research today.

As mentioned previously, the use of SPEs in conjunction with EIS is sparsely reported, in fact the earliest notable contribution is in 2006 by Lu and Chen.[97] In their work, they created SPEs for the sensing of glucose *via* drop coating a mixture of Fe_3O_4 nanoparticles and ferricyanide onto a carbon SPE, after which glucose oxidase was drop coated onto the electrode.[97] Unfortunately EIS was only used in their study to characterise their electrodes, which intriguingly were found to exhibit a larger R_{ct} upon the addition of glucose oxidase.[97] An interesting approach would be to use the generic methodologies seen in this review to study the effect upon R_{ct} of the glucose oxidase and the effect of glucose concentration.

The following year, gold SPEs were fabricated by Balkenhohl and Lisdat as impedimetric immunosensors.[98] The electrodes are coated with a layer of sodium-4-styrensulfonic acid, which acts as an anchor for transglutaminase, which is a molecule associated with the autoimmune disorder celiac disease.[98] After application of the enzyme, bovine serum albumin was applied to the electrode to block non-specific binding sites. The SPE could then be used for the impedimetric detection of anti-transglutaminase antibodies.[98] The Nyquist plots as shown in Fig. 13 compare the different types of antibodies studied, and paying particular attention to curve 1 and 2, it is observed that the immunosensor without anti-transglutaminase (1) exhibits a smaller R_{ct} than the one with the transglutaminase (2). In fact, according to their experimental data, the R_{ct} is over double for the immunosensor incubated with the antibody (39.7 kΩ (1) compared to 97.6 kΩ (2)).[98] In addition to this, concentration studies were performed but unfortunately did not yield a linear calibration plot which would have allowed its use as an analytical sensor.

More recently, Rohrbach and co-workers have developed a screen printed sensor for the detection of lysozyme,[99] an enzyme

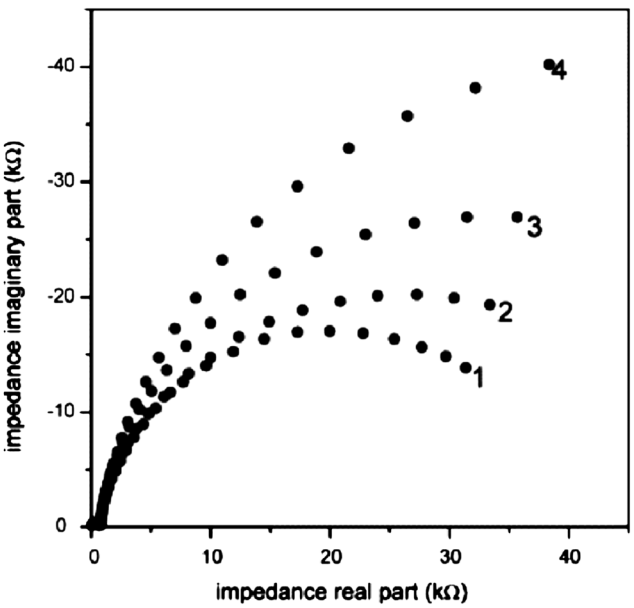

Fig. 13 Nyquist plots of the Faradaic impedance measurements of the screen-printed gold electrodes after the different incubation steps of the assay procedure. Measurements were performed in 10 mM L^{-1} phosphate buffer of pH 7, including 2.5 mM $[Fe(CN)_6]^{3-}$ and 2.5 mM $[Fe(CN)_6]^{4-}$, within a frequency range from 500 to 1000 Hz. (1) Electrode after transglutaminase immobilization and blocking of residual binding sites with bovine serum albumin (2) immunosensor after incubation with an anti-transglutaminase antibody solution. (3) Immunosensor after the incubation with peroxidase-labelled anti-rabbit IgG antibodies (4) immunosensor after the assay procedure (after oxidation of 3-amino-9-ethylcarbazole by peroxidase activity and subsequent precipitation of the product on the electrode surface). Reprinted from ref. 92 with permission from Elsevier.

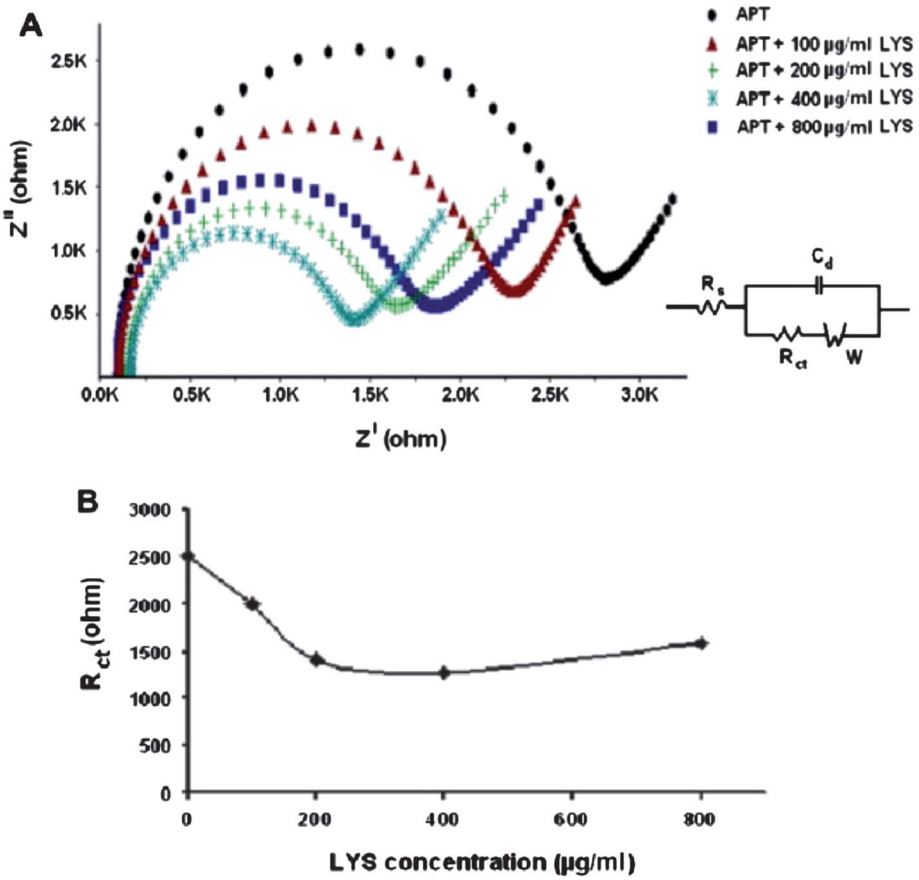

Fig. 14 Nyquist diagrams recorded with supporting electrolyte solution 2.5 mM $K_3[Fe(CN)_6]/K_4[Fe(CN)_6]$ (1 : 1) containing 0.1 M KCl by using MWCNT–SPEs with immobilized 200 µg mL^{-1} aptamer for different LYS concentrations such as 0, 100, 200, 400, and 800 µg mL^{-1}. Reproduced from ref. 93 with permission from Elsevier.

most notably found in tears and egg white and is reported to exhibit cell destruction properties.[100] Carbon nanotube SPEs have been modified with an amino-modified DNA aptamer which recognises lysozyme.[99] The results of concentration studies are presented in Fig. 14 as a Nyquist plot and a plot of concentration *versus* R_{ct}. Fig. 14A shows that the R_{ct} decreases upon lysozyme incubation. The authors state that the R_{ct} levels off above lysozyme concentrations of 400 µg L^{-1} which is represented in Fig. 14B which is not entirely correct as the R_{ct} value gradually increases again; nevertheless % RSD measurements would benefit the work.[99]

There have been further studies utilising SPEs, for instance for the detection of lead using bismuth-modified SPEs,[101] short DNA strand HIV detection utilising carbon SPEs modified with chitosan and Fe_3O_4 nanoparticles,[102] and the detection of *E. Coli* using gold SPEs.[103]

There is evidently a scope of interest within the electrochemical field to apply SPEs and EIS to analytically useful measurements as highlighted in the above examples. It is perfectly reasonable to suggest an interesting line of inquiry would be to apply the techniques towards the sensing of the diseases as highlighted in the previous section with the benefit of screen printed electrodes for the potential use for an on-the-spot, quick and disposable sensing method, avoiding the need for sending samples away for laboratory testing. There are many more exciting examples of EIS for sensing purposes which covers Sections 4, 5, and 6; Table 1 provides an overview of some of these exciting examples for interested readers to explore in more detail.

7 Conclusions

Throughout the history of EIS, there have been many trials and tribulations which have prevented the technique from becoming one that can be used in industrial environments, for instance in the early 1960's the lack of advancement of electronics meant that only single frequencies could be measured in one experiment and as such experiments were cumbersome, if not vastly time consuming.[11] However, we have seen the advancement of the technique now to a point where it is better understood by an increasing number of scientists and further the technique has been used industrially, for example, in the case of corrosion measurements.[11] As observed, EIS is being extensively researched for use with biological platforms and is a technique of choice for many institutions and the technique also being modified now for specific uses such as molecular binding using plasmonic-based EIS.[104] Unfortunately the technique is still not fully understood, specifically by electrochemists (typified by the use of EIS as more of a means of supporting voltammetric evidence for electrochemical work

rather than a primary technique). However, due to the wealth of information available from the use of EIS, there is no doubt that the research community will continue to use and improve their knowledge of the technique and in future it shows a great amount of potential for applications in electroanalysis (particularly as a medicinal technology) as it potentially offers a quicker and cheaper route for detection of target analytes. In particular, if impedimetric technology was applied more to screen printed electrodes, the synergy, utilising the benefits of disposable sensors could be utilised to detect the diseases of, for example, HIV, gonorrhoea and MRSA providing de-centralised clinical testing and also negating lengthy immunoassay/ELISA techniques. Critically, it is shown in Table 1 that EIS is a highly sensitive technique with detection limits as low as the *picomolar* range; the future use of EIS in biological applications looks highly promising.

References

1 E. Warburg, *Ann. Phys. Chem.*, 1899, **67**, 493.
2 W. Nernst, *Z. Elektrochem.*, 1894, **14**, 622.
3 A. Nishikata, Y. Ichihara and T. Tsuru, *Corros. Sci.*, 1995, **37**, 897.
4 F. Mansfield, *Electrochim. Acta*, 1990, **35**, 1533.
5 Q. Mohsen, S. S. Fadl-allah and N. S. El-Shenawy, *Int. J. Electrochem. Sci.*, 2012, **7**, 4510.
6 L. Strašák, J. Dvořák, S. Hasoň and V. Vetterl, *Bioelectrochemistry*, 2002, **56**, 37.
7 P. M. Gomadam and J. W. Weidner, *Int. J. Energy Res.*, 2005, **29**, 1133.
8 Z. He and F. Mansfield, *Energy Environ. Sci.*, 2009, **2**, 215.
9 A. G. Webster, *Proc. Natl. Acad. Sci. U. S. A.*, 1919, **5**, 275.
10 D. D. Macdonald, *Electrochim. Acta*, 2006, **51**, 1376.
11 E. Barsoukov and J. R. Macdonald, *Impedance Spectroscopy: Theory, Experiment, and Applications*, Wiley, 2005.
12 University of St Andrews, http://www-groups.dcs.st-and.ac.uk/~history/Mathematicians/Heaviside.html, accessed November 2012.
13 P. Yang, Q. Zheng, H. Xu, J. Liu and L. Jin, *Chin. J. Chem.*, 2012, **30**, 1155.
14 L. Wang, J. Zhao, X. He, J. Gao, J. Li, C. Wan and C. Jiang, *Int. J. Electrochem. Sci.*, 2012, **7**, 345.
15 D. C. Graham, *Chem. Rev.*, 1947, **41**, 441.
16 K. Jüttner, *Electrochim. Acta*, 1990, **35**, 1501.
17 H. Fricke, *Cold Spring Harbor Symp. Quant. Biol.*, 1933, **1**, 117.
18 F. Lisdat and D. Schäfer, *Anal. Bioanal. Chem.*, 2008, **391**, 1555.
19 C. Alexander and M. Sadiku, *Fundamentals of Electric Circuits*, McGraw-Hill, 2006.
20 B. Hirschorn, I. Ibrahim, M. E. Orazem, H. Takenouti and B. Tribollet, *ECS Trans.*, 2008, **13**, 81.
21 D. A. C. Brownson, A. C. Lacombe, M. Gómez-Mingot and C. E. Banks, *RSC Adv.*, 2012, **2**, 665.
22 E. P. Randviir, D. A. C. Brownson, M. Gómez-Mingot, D. K. Kampouris, J. Iniesta and C. E. Banks, *Nanoscale*, 2012, **4**, 6470.
23 http://www.solartronanalytical.com/Pages/SMaRTSoftware.htm, accessed 11 September 2012.
24 http://www.thasar.com/cms/images/ivium/pdf/ivium_technologies_brochure.pdf, accessed 11 September 2012.
25 J. R. Scully and D. C. Silverman, *Electrochemical impedance: analysis and interpretation*, ASTM International, 1993.
26 J. R. MacDonald, *J. Electroanal. Chem.*, 1987, **223**, 25.
27 H. Wang and L. Pilon, *Electrochim. Acta*, 2012, **63**, 55.
28 F. Lufrano, P. Staiti and M. Minutoli, *J. Power Sources*, 2003, **124**, 314.
29 J. F. Rubinson and Y. P. Kayinamura, *Chem. Soc. Rev.*, 2009, **38**, 3339.
30 J. R. Macdonald, *Impedance Spectroscopy*, John Wiley, 1987.
31 X. Dominguez-Benetton, S. Sevda, K. Vanbroekhoven and D. Pant, *Chem. Soc. Rev.*, 2012, **41**, 7228.
32 J. H. Sluyters and J. J. C. Oomen, *Recl. Trav. Chim. Pays-Bas*, 1960, **79**, 1101.
33 J. H. Sluyters, *Recl. Trav. Chim. Pays-Bas*, 1960, **79**, 1092.
34 R. G. S. Evanston, *US Pat.*, 3607673, 21 September 1971.
35 I. Epelboin, M. Keddam and H. Takenouti, *J. Appl. Electrochem.*, 1972, **2**, 71.
36 F. Mansfield, *J. Appl. Electrochem.*, 1995, **25**, 187.
37 D. Mareci, R. Chelariu, S. Iacoban, C. Munteanu, G. Bolat and D. Sutiman, *J. Mater. Eng. Perform.*, 2012, **21**, 1431.
38 T. Fusayama, T. Katayori and S. Nomoto, *J. Dent. Res.*, 1963, **42**, 1183.
39 J. Pan, D. Thierry and C. Leygraf, *Electrochim. Acta*, 1996, **41**, 1143.
40 D. Xue, Z. Tan, M. J. Schulz, W. J. Vanooij, J. Sankar, Y. Yun and Z. Dong, *Mater. Sci. Eng., C*, 2012, **32**, 1230.
41 G. L. Song and S. Z. Song, *Adv. Eng. Mater.*, 2007, **9**, 298.
42 http://batteryuniversity.com/learn/article/lithium_ion_safety_concerns, accessed 20 July 2012.
43 J. Yan, W. Yuan, Z. Tang, H. Xie, W. Mao and L. Ma, *J. Power Sources*, 2012, **209**, 251.
44 S. Q. Liu, S. C. Li, K. L. Huang, B. L. Gong and G. Zhang, *J. Alloys Compd.*, 2008, **450**, 499.
45 J. X. Ma, C. S. Wang and S. Wroblewski, *J. Power Sources*, 2007, **164**, 849.
46 R. Yazami and Y. Ozawa, *J. Power Sources*, 2006, **153**, 251.
47 K. Dokko, M. Mohamedi, M. Umeda, *et al.*, *J. Electrochem. Soc.*, 2003, **150**, A425.
48 S. Q. Liu, S. C. Li and K. L. Huang, *Chin. J. Inorg. Chem.*, 2006, **22**, 645.
49 X. Yuan, H. Wang, J. C. Sun and J. Zhang, *Int. J. Hydrogen Energy*, 2007, **32**, 4365.
50 J. Wu, X. Z. Yuan, H. Wang, M. Blanco, J. J. Martin and J. Zhang, *Int. J. Hydrogen Energy*, 2008, **33**, 1735.
51 A. P. Borole, D. Aaron, C. Y. Hamilton and C. Tsouris, *Environ. Sci. Technol.*, 2010, **44**, 2740.
52 D. Samanta and A. Sarkar, *Chem. Soc. Rev.*, 2011, **40**, 2567.
53 L. Hlavata, K. Benikova, V. Vyskocil and J. Labuda, *Electrochim. Acta*, 2012, **71**, 134.
54 C. E. Banks, T. J. Davies, G. G. Wildgoose and R. G. Compton, *Chem. Commun.*, 2005, 829.

55 S. Siddiqui, Z. Dai, C. J. Stavis, H. Zeng, N. Moldovan, R. J. Hamers, J. A. Carlisle and P. U. Arumugam, *Biosens. Bioelectron.*, 2012, **35**, 284.
56 G. Zheng, F. Patolsky, Y. Cui, W. U. Wang and C. M. Lieber, *Nat. Biotechnol.*, 2005, **23**, 1294.
57 Y. Cui, Q. Wei, H. Park and C. M. Lieber, *Science*, 2001, **293**, 1289.
58 N. S. Mathebula, J. Pillay, G. Toschi, J. A. Verschoor and K. I. Ozoemena, *Chem. Commun.*, 2009, 3345.
59 K. R. U. Devi, B. Ramalingam and A. Raja, *Diagn. Microbiol. Infect. Dis.*, 2003, **46**, 205.
60 G. Liu, S. G. Iyengar and J. J. Gooding, *Electroanalysis*, 2012, **24**, 1509.
61 M. Wang, Q. Sheng, D. Zhang, Y. He and J. Zheng, *Bioelectrochemistry*, 2012, **86**, 46.
62 A. Mokhtari, H. Karimi-Maleh, A. A. Ensafi and H. Beitollahi, *Sens. Actuators, B*, 2012, **169**, 96.
63 S. R. Santos and G. Maia, *Electrochim. Acta*, 2012, **71**, 116.
64 L. B. Venarusso, K. Tammeveski and G. Maia, *Electrochim. Acta*, 2011, **56**, 8926.
65 E. Prats-Alfonso, X. Sisquella, N. Zine, G. Gabriel, A. Guimerà, F. J. Del Campo, R. Villa, A. H. Mrksich, A. Errachid, J. Aquiló and F. Albericio, *Small*, 2012, **8**, 2106.
66 E. E. Ferapontova and K. V. Gothelf, *Curr. Org. Chem.*, 2011, **15**, 498.
67 The Nobel Prize in Physics 2010, Nobelprize.org, 25 September 2012 http://www.nobelprize.org/nobel_prizes/physics/laureates/2010/.
68 K. S. Novoselov, D. Jiang, F. Schedin, T. J. Booth, V. V. Khotkevich, S. V. Morozov and A. K. Geim, *Proc. Natl. Acad. Sci. U. S. A.*, 2005, **102**, 10451.
69 D. A. C. Brownson, D. K. Kampouris and C. E. Banks, *Chem. Soc. Rev.*, 2012, **41**, 6944.
70 E. P. Randviir and C. E. Banks, *RSC Adv.*, 2012, **2**, 5800.
71 D. A. C. Brownson, L. J. Munro, D. K. Kampouris and C. E. Banks, *RSC Adv.*, 2011, **1**, 978.
72 D. A. C. Brownson, J. P. Metters, D. K. Kampouris and C. E. Banks, *Electroanalysis*, 2011, **23**, 894.
73 A. J. Bard, *J. Chem. Educ.*, 1983, **60**, 302.
74 C. D. Bain, J. Evall and G. M. Whitesides, *J. Am. Chem. Soc.*, 1989, **111**, 7155.
75 R. G. Nuzzo and D. L. Allara, *J. Am. Chem. Soc.*, 1983, **105**, 4481.
76 M. D. Porter, T. B. Bright, D. L. Allara and C. E. D. Chidsey, *J. Am. Chem. Soc.*, 1987, **109**, 3559.
77 A. Bonanni, M. I. Pividori and M. del Valle, *Analyst*, 2010, **135**, 1765.
78 A. Bonanni, M. J. Esplandiu and M. del Valle, *Biosens. Bioelectron.*, 2009, **24**, 2885.
79 H. L. Poh, A. Bonanni and M. Pumera, *RSC Adv.*, 2012, **2**, 1021.
80 A. Bonanni, A. H. Loo and M. Pumera, *Trends Anal. Chem.*, 2012, **37**, 12.
81 Z. Wang, J. Zhang, P. Chen, X. Zhou, Y. Yang, S. Wu, L. Niu, Y. Han, L. Wang, P. Chen, F. Boey, Q. Zhang, B. Liedberg and H. Zhang, *Biosens. Bioelectron.*, 2011, **26**, 3881.
82 M. Giovanni, A. Bonanni and M. Pumera, *Analyst*, 2012, **137**, 580.
83 A. Bonanni and M. Pumera, *ACS Nano*, 2011, **5**, 2356.
84 A. H. Loo, A. Bonanni and M. Pumera, *Nanoscale*, 2012, **4**, 143.
85 A. H. Loo, A. Bonanni, H. L. Poh and M. Pumera, *Nanoscale*, 2012, **4**, 921.
86 R. K. S. Raman, P. C. Banerjee, D. E. Lobo, H. Gullapalli, M. Sumandasa, A. Kumar, L. Choudhary, R. Tkacz, P. M. Ajayan and M. Majumder, *Carbon*, 2012, **50**, 4040.
87 D. Prasai, J. C. Tuberquia, R. R. Harl, G. K. Jennings and K. I. Bolotin, *ACS Nano*, 2012, **6**, 1102.
88 Y. Yuan, S. Zhou, B. Zhao, L. Zhuang and Y. Wang, *Bioresour. Technol.*, 2012, **116**, 453.
89 P. Liang, H. Wang, X. Xia, X. Huang, Y. Mo, X. Cao and M. Fan, *Biosens. Bioelectron.*, 2011, **26**, 3000.
90 Y. Hu, F. Li, X. Bai, D. Li, S. Hua, K. Wang and L. Niu, *Chem. Commun.*, 2011, **47**, 1743.
91 R. Singh, Z. Matharu, A. K. Srivastava, S. Sood, R. K. Gupta and B. D. Malhotra, *Microchim. Acta*, 2012, **177**, 201.
92 Z. Wang, X. Zhou, J. Zhang, F. Boey and H. Zhang, *J. Phys. Chem. C*, 2009, **113**, 14071.
93 J. P. Metters, R. O. Kadara and C. E. Banks, *Analyst*, 2011, **136**, 1067.
94 J. P. Metters, F. Tan, R. O. Kadara and C. E. Banks, *Anal. Methods*, 2012, **4**, 1272.
95 R. O. Kadara, N. Jenkinson and C. E. Banks, *Electrochem. Commun.*, 2009, **11**, 1377.
96 M. Khairy, R. O. Kadara and C. E. Banks, *Anal. Methods*, 2010, **2**, 851.
97 B. Lu and W. Chen, *J. Magn. Magn. Mater.*, 2006, **304**, e400.
98 T. Balkenhohl and F. Lisdat, *Anal. Chim. Acta*, 2007, **597**, 50.
99 F. Rohrbach, H. Karadeniz, A. Erdem, M. Famulok and G. Mayer, *Anal. Biochem.*, 2012, **421**, 454.
100 K. Yoshimura, A. Toibana and K. Nakahama, *Biochem. Biophys. Res. Commun.*, 1988, **150**, 794.
101 J. C. Quintana, F. Arduini, A. Arnine, F. Punzo, G. Li Destri, C. Bianchini, D. Zane, A. Curulli, G. Palleschi and D. Moscone, *Anal. Chim. Acta*, 2011, **707**, 171.
102 L. Tran, B. Nguyen, N. Hieu, H. Tran, H. Nguyen and P. Nguyen, *Mater. Sci. Eng., C*, 2011, **31**, 477.
103 V. Gómez, S. Campuzano, M. Pedrero and J. M. Pingarrón, *Biosens. Bioelectron.*, 2009, **24**, 3365.
104 J. Lu, W. Wang, S. Wang, X. Shan, J. Li and N. Tao, *Anal.Chem.*, 2012, **84**, 327.
105 T. Yang, N. Zhou, Q. Li, Q. Guan, W. Zhang and K. Jiao, *Colloids Surf., B*, 2012, **97**, 150.
106 A. Erdem, M. Muti, H. Karadeniz, G. Congur and E. Canavar, *Colloids Surf., B*, 2012, **95**, 222.
107 A. Gasnier, M. L. Pedano, F. Gutierrez, P. Labbé, G. A. Rivas and M. D. Rubianes, *Electrochim. Acta*, 2012, **71**, 73.
108 Y. Liu, Y. Liu, H. Feng, Y. Wu, L. Joshi, X. Zeng and J. Li, *Biosens. Bioelectron.*, 2012, **35**, 63.
109 D. Zhang, F. Zhang, Y. Cui, Q. Deng, S. Krause, Y. Zhou and X. Zhang, *Talanta*, 2012, **92**, 65.
110 L. Shi, G. Liang, X. Li and X. Liu, *Anal. Methods*, 2012, **4**, 1036.

111 Y. Li and S. Chen, *Int. J. Electrochem. Sci.*, 2012, **7**, 2175.
112 X. Guo, A. Kulkarni, A. Doepke, H. B. Halsall, S. Iyer and W. R. Heineman, *Anal. Chem.*, 2012, **84**, 241.
113 M. Venugopal, S. K. Arya, G. Chornokur and S. Bhansali, *Sens. Actuators, A*, 2011, **172**, 154.
114 T. L. Adamson, F. A. Eusebio, C. B. Cook and J. T. Labelle, *Analyst*, 2012, **137**, 4179.
115 I. Ciani, H. Schulze, D. K. Corrigan, G. Henihan, G. Giraud, J. G. Terry, A. J. Walton, R. Pethig, P. Ghazal, J. Crain, C. J. Campbell, T. T. Bachmann and A. R. Mount, *Biosens. Bioelectron.*, 2012, **31**, 413.
116 Q. Li, W. Cheng, D. Zhang, T. Yu, Y. Yin, H. Ju and S. Ding, *Int. J. Electrochem. Sci.*, 2012, **7**, 844.
117 H. Xu, L. Wang, H. Ye, L. Yu, X. Zhu, Z. Lin, G. Wu, X. Li, X. Liu and G. Chen, *Chem. Commun.*, 2012, **48**, 6390.
118 L. C. Z. Lin, G. Zhang, Q. Liu, B. Qiu, Z. Cai and G. Chen, *Analyst*, 2012, **137**, 819.
119 J. Liang, B. Chen and Y. Long, *Analyst*, 2011, **136**, 4053.
120 A. A. Ensafi, M. Taei, H. R. Rahmani and T. Khayamian, *Electrochim. Acta*, 2011, **56**, 8176.
121 L. Yang, Y. Li, C. L. Griffis and M. G. Johnson, *Biosens. Bioelectron.*, 2004, **19**, 1139.
122 L. Yang, C. Ruan and Y. Li, *Biosens. Bioelectron.*, 2003, **19**, 495.
123 Y. Hou, S. Helali, A. Zhang, N. Jaffrezic-Renault, C. Martelet, J. Minic, T. Gorojankina, M. Persuy, E. Pajot-Augy, R. Salesse, F. Bessueille, J. Samatier, A. Errachid, V. Akimov, L. Reggiani, C. Pennetta and E. Alfinito, *Biosens. Bioelectron.*, 2006, **21**, 1393.
124 F. Darain, D. Park, J. Park and Y. Shim, *Biosens. Bioelectron.*, 2004, **19**, 609.
125 G. Liu, J. Liu, T. P. Davis and J. J. Gooding, *Biosens. Bioelectron.*, 2011, **26**, 3660.
126 M. Grossi, M. Lanzoni, A. Pompei, R. Lazzarini, D. Matteuzzi and B. Riccò, *Biosens. Bioelectron.*, 2008, **23**, 1616.
127 R. Pei, Z. Cheng, E. Wang and X. Yang, *Biosens. Bioelectron.*, 2001, **16**, 355.
128 T. V. da Silva Santos, R. R. Teixeira, D. L. Franco, J. M. Madurro, A. C. Brito-Madurro and F. S. Espindola, *Mater. Sci. Eng., C*, 2012, **32**, 530.
129 Y. Chen, C. Wu, J. Tsai and G. Wang, *Int. J. Nanomed.*, 2012, **7**, 133.
130 R. Devi, S. Yadav and C. S. Pundir, *Analyst*, 2012, **137**, 154.
131 A. Lund, T. Jacobsen, K. V. Hansen and M. Mogensen, *Sens. Actuators, B*, 2011, **160**, 1159.
132 N. Meini, R. Kherrat and N. Jaffrezic-Renault, *Sens. Lett.*, 2011, **9**, 2127.
133 B. Khadro, A. Betatache, C. Sanglar, A. Bonhomme, A. Errachid and N. Jaffrezic-Renault, *Sens. Lett.*, 2011, **9**, 2261.
134 S. Zougar, O. Bechiri, S. Baali, R. Kherrat, M. Abbessi, N. Jaffrezic-Renault and N. Fertikh, *Sens. Lett.*, 2011, **9**, 2287.
135 B. B. Narakathu, W. Guo, S. O. Obare and M. Z. Atashbar, *Sens. Lett.*, 2011, **158**, 69.
136 V. Vermeeren, L. Grieten, N. V. Bon, N. Bijnens, S. Wenmackers, S. D. Janssens, K. Haenen, P. Wagner and L. Michiels, *Sens. Actuators, B*, 2011, **157**, 130.
137 Z. Lin, X. Li and H. Kraatz, *Anal. Chem.*, 2011, **83**, 6896.
138 S. Qiu, S. Gao, Q. Liu, Z. Lin, B. Qiu and G. Chen, *Biosens. Bioelectron.*, 2011, **26**, 4326.
139 B. B. Narakathu, M. Z. Atashbar and B. Bejcek, *Sens. Lett.*, 2011, **9**, 872.
140 B. B. Narakathu, M. Z. Atashbar and B. E. Bejcek, *Biosens. Bioelectron.*, 2010, **26**, 923.
141 D. T. Tran, V. Vermeeren, L. Grieten, S. Wenmackers, P. Wagner, J. Pollet, K. P. F. Janssen, L. Michiels and J. Lammertyn, *Biosens. Bioelectron.*, 2011, **26**, 2987.
142 S. Roy, N. Soin, R. Bajpai, D. S. Misra, J. A. McLaughlin and S. S. Roy, *J. Mater. Chem.*, 2011, **21**, 14725.
143 A. Bonanni, M. Pumera and Y. Miyahara, *Phys. Chem. Chem. Phys.*, 2011, **13**, 4980.
144 S. Bourigua, M. Hnaien, F. Bessueille, F. Lagarde, S. Dzyadevych, A. Maaref, J. Bausells, A. Errachid and N. Jaffrezic-Renault, *Biosens. Bioelectron.*, 2010, **26**, 1278.
145 P. R. Solanki, A. Kaushik, T. Manaka, M. K. Pandey, M. Iwamoto, V. V. Agrawal and B. D. Malhotra, *Nanoscale*, 2010, **2**, 2811.
146 J. Park, Y. Lee, B. Chang, B. H. Kim, S. Jeon and S. Park, *Anal. Chem.*, 2010, **82**, 9342.
147 V. Pasceri, J. T. Willerson and E. T. Yeh, *Circulation*, 2000, **102**, 2165.